Quantifying Renal Perfusion at 3 T and 0.6 T using Arterial Spin Labeling MRI

W. Deen



Quantifying Renal Perfusion at 3 T and 0.6 T using Arterial Spin Labeling MRI

W. Deen

Submitted in partial fulfilment of the requirements for the degree of ${\it Master~of~Science}~{\rm in~Biomedical~Engineering}$ ${\it Track:~Medical~Devices}$

at the Delft University of Technology to be defended publicly on 12/11/2025 at 10:30

Thesis advisor: Dr. Rob Remis

Thesis committee:

Dr. Rob Remis (Chair), Dr. Sebastian Weingärtner, Dr. Maša Božić-Iven

Abstract

Objective: The aim of this project is to quantify renal perfusion at 3 T with arterial spin labeling (ASL) images and to evaluate the feasibility of this measurement at 0.6 T.

Background: Chronic kidney disease (CKD) affects over one in ten individuals worldwide and has a high mortality rate. As renal microvascular dysfunction plays a key role in CKD progression, accurate and non-invasive quantification of renal perfusion is valuable. ASL magnetic resonance imaging (MRI) enables the measurement of renal perfusion without exogenous contrast agents and has been validated at 1.5 T and 3 T. However, its feasibility at 0.6 T has not yet been investigated.

Methodology: Data from the NEO-2 study acquired at 3 T was analyzed using a pipeline that included image registration, segmentation, and quantitative perfusion mapping. Midfield scanners have a lower signal-to-noise ratio and altered relaxation times. Therefore, the existing renal ASL sequence used in 3 T was adjusted. The sequence parameters that were modified included the repetition time (TR), the number of control-label pairs, voxel size, post-label delay (PLD), and background suppression (BGS) pulse timings. After choosing the optimal parameters, a healthy volunteer was scanned back-to-back at both field strengths for direct comparison.

Results: At 3 T, cortical perfusion values ranged between 180 and 286 mL/100 g/min, consistent with literature. Optimal parameters at 0.6 T were: TR = 4000 ms, 25 control–label pairs, in-plane resolution of 4×4 mm 2 , slice thickness of 10 mm, and PLD = 1400 ms with BGS pulses at 700 & 1100 ms. With these settings applied at 0.6 T, the cortical perfusion values were 215.34 ± 67.92 and 236.80 ± 66.33 mL/100 g/min in the left and right cortex, respectively. Using the 3 T acquisition protocol, the corresponding values were 241.89 ± 76.55 and 250.75 ± 70.82 mL/100g/min, respectively. Values at 3 T were approximately 5–10% higher.

Conclusion: The results show that renal ASL at 0.6 T can produce quantitative perfusion estimates that are similar to those at 3 T.

Table of Contents

\mathbf{A}	bstra	ct		ii
Li	st of	Table	5	\mathbf{v}
Li	st of	Figure	es	vi
Li	st of	Abbre	eviations	viii
\mathbf{A}	ckno	wledge	ements	ix
1	Intr	roducti	ion	1
2	The	eoretic	al Background	4
	2.1	Anato	my of the kidney	4
	2.2	Magne	etic Resonance Imaging	6
		2.2.1	Behavior of Nuclei in a Magnetic Field	6
		2.2.2	Excitation and Signal Detection	7
		2.2.3	Spatial Encoding and Image Reconstruction	8
		2.2.4	Readout methods	8
	2.3	Arteri	al Spin Labeling (ASL) MRI	10
	2.4	Mid-fi	eld MRI	11
		2.4.1	Advantages	11
		2.4.2	Challenges and parameter adjustments	12
3	Met	thods		14
	3.1	Renal	Perfusion Quantification at 3 T	14
		3.1.1	Analysis Pipeline for 3 T Dataset	15
			3.1.1.1 Registration	17
			3.1.1.2 Segmentation	17
			3.1.1.3 Quantification	18
		3.1.2	Heidelberg 2020 vs. Current Pipeline	18

	3.2	Renal	Perfusion Quantification at 0.6 T	19
		3.2.1	Acquisition	19
			3.2.1.1 Control–Label Pairs and Repetition Time (TR)	20
			3.2.1.2 In-Plane Resolution and Slice Thickness	20
			3.2.1.3 PLD and BGS pulses	20
		3.2.2	Analysis Pipeline 0.6 T	21
4	Res	ults		22
	4.1	Renal	Perfusion Results at 3 T	22
	4.2	Renal	Perfusion Results at 0.6 T	23
		4.2.1	Repetition Time (TR) and Control-Label Pairs	24
		4.2.2	In-Plane Resolution and Slice Thickness	25
		4.2.3	Post Label Delay (PLD)	27
		4.2.4	Background Suppression (BGS) pulses	27
		4.2.5	Post-processing	28
			4.2.5.1 Registration	28
			4.2.5.2 Segmentation	28
	4.3	Comp	arison of Renal Perfusion at 3 T and 0.6 T	29
5	Disc	cussion	ı	32
	5.1	Renal	Perfusion Results at 3 T	32
	5.2	Renal	Perfusion Results at 0.6 T	33
	5.3	Comp	arison of Renal Perfusion Results at 3 T and 0.6 T	35
6	Con	clusio	n	37
Bi	bliog	graphy		38
\mathbf{A}	Par	ametei	Text File	43
В	$\operatorname{Lit}_{oldsymbol{\epsilon}}$	erature	Review	45

List of Tables

3.1	FAIR-ASL and M_0 acquisition parameters at 3 T	15
3.2	Differences between Heidelberg and current pipeline	19
3.3	FAIR-ASL parameters changed for the 0.6 T MRI scanner	19
4.1	Mean cortical perfusion values at 3 T	22
4.2	Mean cortical perfusion values at 3 T and 0.6 T	30

List of Figures

2.1	Coronal CT slice of kidneys	4
2.2	Kidney anatomy	5
2.3	Comparison of magnetic and non-magnetic nuclei	6
2.4	Fundamental properties of the hydrogen nucleus	6
2.5	Free induction decay	7
2.6	Spin echo pulse sequence	8
2.7	Gradient echo pulse sequence	9
2.8	Echo-planar imaging pulse sequence	9
2.9	Positioning for pCASL and FAIR	11
3.1	Renal perfusion quantification workflow	16
3.2	Registration effect on PWI	17
3.3	Renal segmentation workflow	18
4.1	Renal perfusion maps	23
4.2	First MR images at 0.6 T	23
4.3	Perfusion-weighted images at different TRs	24
4.4	Manual segmentation of cortical ROI	24
4.5	Perfusion-weighted images with tSNR values	25
4.6	Comparison of in-plane resolution	25
4.7	Comparison of left kidney in-plane resolutions	26
4.8	Comparison of slice thickness	26
4.9	PLD and BGS timings	27
4.10	Comparison of BGS timings	27
4.11	Effect of registration on PWI	28
4.12	Erroneous T_1 map at 0.6 T	29
4.13	MR images at 3 T	29
4.14	MR images at 0.6 T	29
1 15	tSNR mans at 3 T and 0.6 T	30

4.16 Comparison of perfusion maps at 3 T and 0.6 T	31
--	----

List of Abbreviations

ASL	Arterial Spin Labeling
B_0	Static Magnetic Field
B_1	Radiofrequency Magnetic Field
BGS	Background Suppression
CKD	Chronic Kidney Disease
EPI	Echo Planar Imaging
FAIR	Flow-sensitive Alternating Inversion Recovery
FFE	Fast Field Echo
FID	Free Induction Decay
FOV	Field of View
GRE	Gradient Recalled Echo
M_0	Fully Relaxed Magnetization Image
MOLLI	Modified Look-Locker Inversion Recovery
MRI	Magnetic Resonance Imaging
NEO-2	Nederlandse Epidemiologie van Obesitas 2
PASL	Pulsed Arterial Spin Labeling
PWI	Perfusion-Weighted Image
pCASL	Pseudo-Continuous Arterial Spin Labeling
PLD	Post-Labeling Delay
QUIPSS-II	Quantitative Imaging of Perfusion using a Single Subtraction, version II
RF	Radiofrequency
ROI	Region of Interest
SNR	Signal-to-Noise Ratio
SPIR	Spectral Presaturation with Inversion Recovery
tSNR	Temporal Signal-to-Noise Ratio
TE	Echo Time
TI	Inversion Time
TI_1	Effective Bolus Duration
TR	Repetition Time

Acknowledgements

Completing this thesis marks the end of my Master of Science in Biomedical Engineering at Delft University of Technology! During this graduation project, I gained a great deal of knowledge and practical experience in the field of renal MRI, especially in image post-processing. This work would not have been possible without the expertise and support of many people, whom I would like to thank.

First, I would like to thank Dr. Rob Remis. I am very grateful for your guidance throughout this project. Your positivity and encouragement have kept me motivated and confident in my work!

My thanks also go to I. Dekkers for the opportunity to undertake my thesis at LUMC and for all the medical discussions alongside B. Siadari.

Special warm thanks to M. Nagtegaal, E. Roefs, T. van Osch, and their wonderful group, whom I could always turn to with any technical problems. I am also very grateful to A. Cernicancu for helping me fill in the gaps related to the Philips data.

I am very thankful to F. Zollner and his group at the University of Heidelberg for making our collaboration possible. Thanks to this, I have managed to make much more progress in this project.

I am especially grateful to M. Božić for being available from the very beginning. Your generous guidance helped me understand a field that was entirely unfamiliar to me at first.

Last but not least, I want to thank my brother for all the insightful discussions and support.

To the thesis committee, thank you for taking the time to review my work. I hope you enjoy reading this thesis.

Best, Willemijn

CHAPTER 1

Introduction

Chronic Kidney Disease (CKD) affects more than one in ten individuals worldwide and has a high mortality rate [1]. Estimates suggest that by 2040, CKD may be responsible for 2.2 to 4.0 million deaths, potentially becoming the 5th highest cause of years of life lost globally [2, 3]. CKD is characterized by a decline in renal function, disrupting the kidney's ability to filter blood, maintain homeostasis, and regulate fluid balance. Impaired renal function also increases the risk of cardiovascular disease. In fact, deaths from CKD and cardiovascular complications linked to renal dysfunction account for 4.6% of global mortality [1].

A key pathophysiological mechanism linking renal and cardiovascular disease is microvascular dysfunction [4, 5, 6]. In the kidney, this dysfunction results in reduced perfusion and oxygen delivery, which contribute to tissue hypoxia, inflammation, and consequently progressive loss of renal function. Among all organs in the human body, the kidneys receive between 20% and 25% of the total cardiac output, which is the highest blood flow per gram of tissue [7]. Despite this high perfusion, their complex vascular structure and high oxygen demand make them particularly vulnerable to microvascular injury.

Several studies have reported reduced cortical perfusion in patients with CKD [8, 9, 10], and a variation of this metric depending on the disease stage [11]. The latter suggests that renal perfusion is not only a marker for kidney health, but may also provide insights into disease progression. Therefore, methods to accurately measure this perfusion would be valuable, especially at the early stages of renal diseases.

A variety of imaging techniques have been used to assess renal perfusion, including positron emission tomography (PET), computed tomography (CT), and magnetic resonance imaging (MRI). However, as these techniques have limitations, there is still no gold standard technique available for quantifying renal perfusion in clinical settings. PET and CT expose patients to ionizing radiation, whereas MRI is a radiation-free alternative.

Several MRI techniques have been used to measure renal perfusion, including dynamic contrast-enhanced (DCE) imaging, arterial spin labeling (ASL), and intravoxel incoherent motion diffusion-weighted imaging (IVIM-DWI) [12, 13, 14]. The quantification of renal perfusion with these MRI methods has demonstrated promising results in detecting kidney dysfunction [12, 15, 16, 17]. ASL-MRI is an MRI technique that magnetically labels arterial blood water using radiofrequency (RF) inversion pulses. Unlike other MRI techniques, this technique is non-invasive as it uses an endogenous tracer, which means no contrast agent is required. This characteristic is particularly advantageous for patients with compromised kidney function, who may be at increased risk for complications associated with contrast agent administration, such as nephrogenic systemic fibrosis (NSF) [18, 19]. Moreover, ASL-MRI can provide structural and regional information on renal perfusion. This capability can be relevant in certain cases such as renal transplants, where ASL can detect possible localized dysfunction [20]. As part of the preliminary phase of this thesis, a literature review was conducted to compare ASL with other MRI perfusion techniques. This review provided essential background knowlegde on renal perfusion quantification with ASL-MRI and can be found in Appendix B.

Currently, many studies have been conducted on MRI scanners at 1.5 and 3 T field strength. A recent international consensus panel published technical recommendations to promote methodological consistency in renal ASL methodology at 1.5 and 3 T [20]. This thesis aims to contribute to the standardization of ASL for perfusion quantification of the kidneys. The first part of this project focuses on implementing a renal ASL analysis pipeline at 3 T and applying it to an existing dataset from the Leiden University Medical Centre (LUMC). This pipeline is generated by adapting an existing workflow from the University of Heidelberg. By validating this pipeline on 3 T data, a reliable processing baseline is developed.

While the current state-of-the-art in renal ASL is at 1.5 T and 3 T, there is a growing interest in mid-field MRI systems for certain applications. 0.55-0.6 T scanners have been introduced with the idea to be cheaper, safer, have a smaller footprint, and improve patient comfort due to reduced noise and increased space [21, 22]. A recent study has shown that an MRI at 0.55 T can achieve diagnostic performance comparable to 1.5 T in certain tasks, which indicates that mid-field MRI could be a potential alternative [23]. Moreover, susceptibility artefacts are reduced at lower field strengths, which will be explained in more detail in the next chapter. However, a reduction in field strength decreases the magnetization, resulting in lower signal intensity and, consequently, a reduced signal-to-noise ratio (SNR). Therefore, the second part of this thesis examines whether renal perfusion quantification is achievable at 0.6 T. The same post-processing pipeline developed for the existing 3 T data will be refined and applied to the 0.6 T dataset. By comparing the results across these two field strengths, this work aims to evaluate the feasibility of renal perfusion quantification at 0.6 T.

To summarize, this thesis aims to contribute to the standardization and progress of ASL-MRI for renal perfusion quantification with the following three projects:

1. Implementation and validation of a renal ASL analysis pipeline at 3 T.

The first project focuses on the post-processing of the existing NEO-2 dataset to quantify the renal perfusion values using a workflow adapted from the University of Heidelberg. This step lays the foundation for a reliable pipeline for renal ASL at 0.6 T.

2. Acquisition and optimization of ASL data at 0.6 T.

The second project involves acquiring ASL-MRI data at 0.6 T and choosing the optimal parameters for the quantification of renal perfusion at this field strength.

3. Comparison of renal perfusion results between 3 T and 0.6 T.

The third project compares the MR images, perfusion maps, and quantified values between 3 T and 0.6 T to assess the feasibility of renal perfusion measurement at lower magnetic field strengths.

This thesis is structured as follows. Chapter 2 provides a theoretical background, including renal anatomy and the basic principles of MRI and ASL-MRI. Chapter 3 describes the post-processing pipeline developed for 3 T data and the adjustments made for its application at 0.6 T. Chapter 4 presents the results, including a perfusion map and quantified perfusion values at 3 T, perfusion weighted images with adjusted acquisition parameters for 0.6 T, and a comparison of the perfusion maps and measurements between these two field strengths. Finally, Chapter 5 discusses the findings along with the overall conclusions, limitations, and some recommendations for future research. Parts of this work have been submitted to two international conferences: the European Society of Radiology (ESR) 2026 and the International Society for Magnetic Resonance in Medicine (ISMRM) 2026.

Chapter 2

Theoretical Background

This chapter explains the anatomical and technical background needed to understand this thesis. First, the anatomy of the kidney will be illustrated briefly. In the second part, the basic principles of magnetic resonance imaging (MRI) and the specifics of the ASL technique central to this thesis, PASL-FAIR, will be explained. Finally, the advantages and challenges of a lower MRI field will be discussed.

2.1 Anatomy of the kidney

The kidneys are bean-shaped organs located on either side of the spine. Each kidney has a renal cortex and medulla, which together form the renal parenchyma. On the medial side of each kidney is an indented region called the renal hilum, through which the renal artery enters and the renal vein and ureter exit. The renal pelvis, located within the hilum, is a funnel-shaped cavity that collects urine from the kidney before passing it into the ureter. Figure 2.1 shows a coronal section of the kidneys in a CT scan. The cortex appears as the outer layer, and the medulla is the inner region.

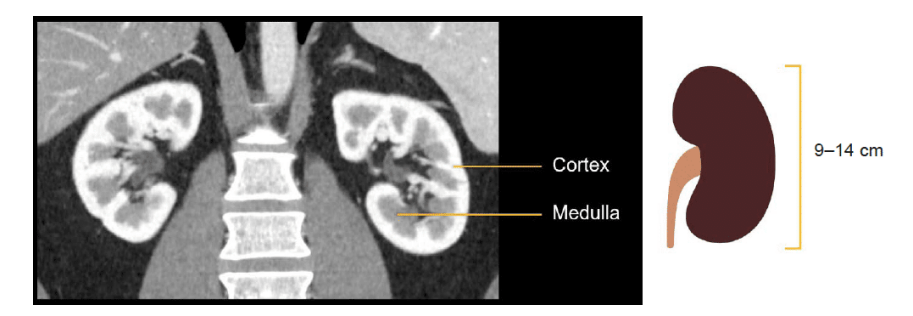


Figure 2.1: Coronal CT slice showing the renal cortex and medulla.

On the medial aspect of the kidney is an indentation known as the renal hilum, through which the renal artery enters and the renal vein and ureter exit. Within the hilum lies the renal pelvis, a funnel-shaped cavity that collects urine from the kidney and channels it into the ureter for transport to the urinary bladder. Each kidney contains around one million filtering units called nephrons. A nephron contains a renal corpuscle and a renal tubule. The renal corpuscle is the component that filters the blood and is located in the cortex. The blood is filtered in the glomerulus, which is a knot of blood capillaries, and is enclosed by the Bowman's capsule (see Figure 2.2). The filtrate from the glomerulus enters the renal tubule, which has segments that extend into the medulla and return to the cortex. The filtered fluid is further processed in the renal tubule through reabsorption and secretion and subsequently forms urine. Figure 2.2 also shows the different segments of the nephron containing the glomeruli, the proximal and distal tubules, the straight part of the proximal tubule (Henle's loop), and part of the collecting system. The medulla contains portions of tubules and fewer capillaries, explaining the significantly lower perfusion compared to the cortex.

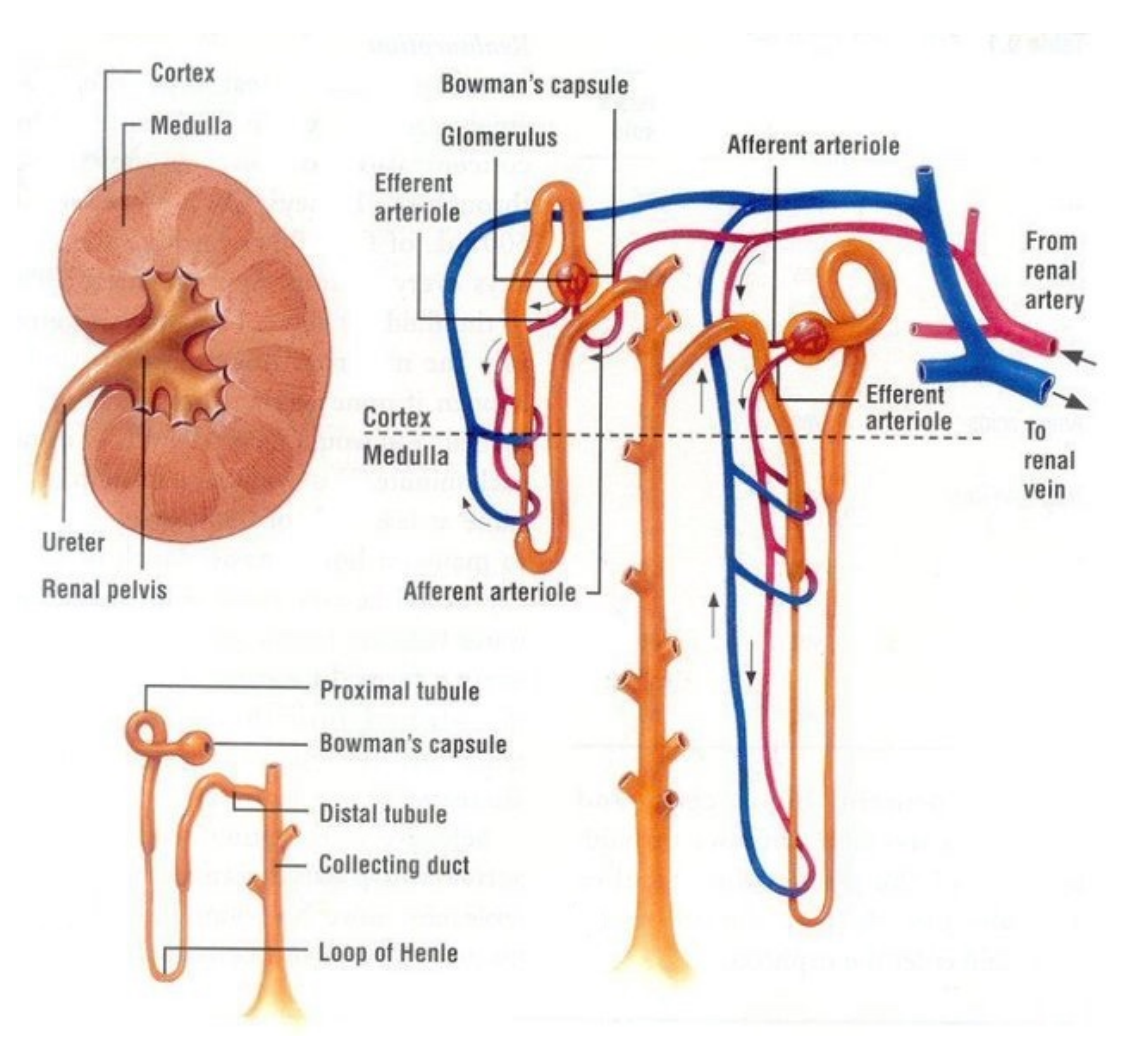


Figure 2.2: Illustration of the kidney anatomy, including nephron segments and their vascular connections.

2.2 Magnetic Resonance Imaging

Magnetic Resonance Imaging (MRI) is an imaging technique that uses nuclear magnetic properties of certain atoms to produce images of tissue. In biological tissues, hydrogen atoms are abundant. Each hydrogen nucleus consists of a single proton, which has an intrinsic property called nuclear spin (I). This spin generates a tiny magnetic field, known as a magnetic moment. When a nucleus has an odd number of protons, the magnetic moments of this nucleus results in a net non-zero spin, as shown in Figure 2.3.

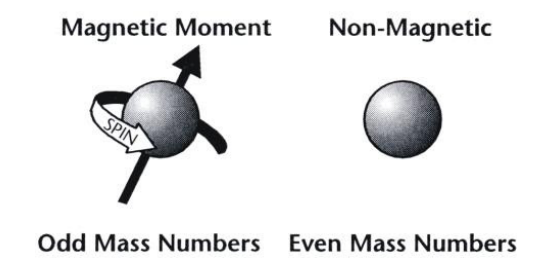


Figure 2.3: Comparison of magnetic and non-magnetic nuclei.

2.2.1 Behavior of Nuclei in a Magnetic Field

In the absence of any external field, the magnetic moments of protons are oriented randomly. By applying an external static magnetic field B_0 , proton spins align to create a net magnetization along the field, see Figure 2.4a. These spins also precess at the Larmor frequency around the B_0 axis, as shown in Figure 2.4b. This Larmor frequency, or resonance frequency, is denoted by ω_0 and directly proportional to B_0 :

$$\omega_0 = \gamma B_0 \tag{2.1}$$

where γ is the gyromagnetic ratio of the nucleus.

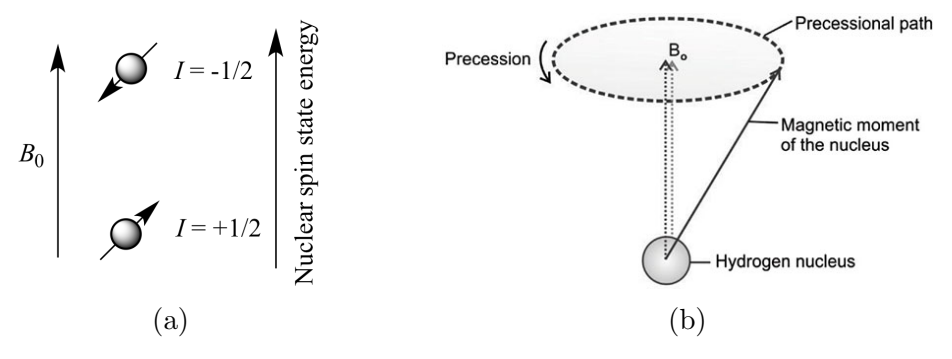


Figure 2.4: Fundamental properties of the hydrogen nucleus. (a) Nuclear spin energy states in a static magnetic field and (b) precession of the magnetic moment around the B_0 axis.

2.2.2 Excitation and Signal Detection

Under equilibrium conditions, the net magnetization of the protons points along the +z direction (along B_0) and produces no measurable signal in the MRI coils. To generate a signal, the magnetization needs to be tipped away from the z-axis into the transverse plane (the xy-plane). This is achieved by applying a radiofrequency (RF) pulse at the Larmor frequency perpendicular to B_0 . This pulse causes the net magnetization to be tipped away with a certain flip angle (α). After excitation, the spins return to equilibrium through two relaxation processes: T_1 (spin-lattice) and T_2 (spin-spin) relaxation. The longitudinal relaxation (T_1) describes the recovery of magnetisation along the main magnetic field B_0 (z-axis), while transverse relaxation (T_2) describes the decay of magnetization due to dephasing interactions in the xy-plane perpendicular to B_0 . The MRI receiver coils can detect the attenuation of the rotating transverse magnetization, known as the free induction decay (FID). This FID decays according to the T_2 relaxation time, which is the combined effect of T_2 relaxation and additional dephasing caused by local magnetic field inhomogeneities (see Figure 2.5). The FID signal contains amplitude and phase information, which is essential for image reconstruction.

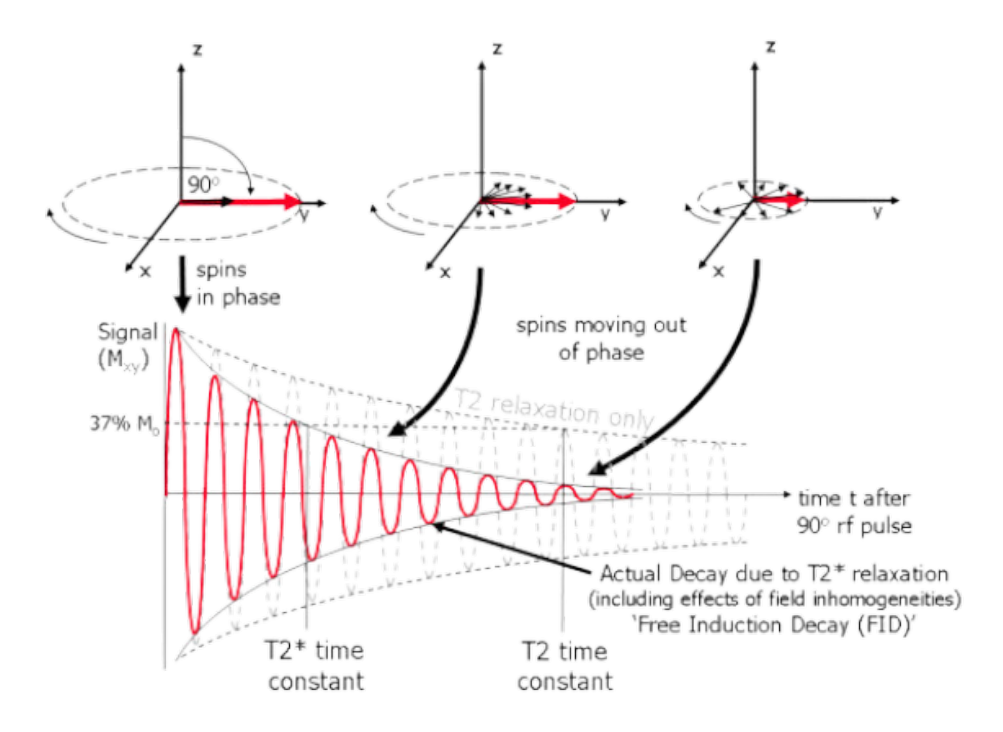


Figure 2.5: Illustration of the free induction decay (FID) due to spin dephasing and T_2 relaxation.

2.2.3 Spatial Encoding and Image Reconstruction

The FID signal is the collective signal from all excited spins and therefore does not contain any spatial information. To create an image from this signal, MRI uses magnetic field gradients in all three spatial directions. These gradients create spatial variations in the Larmor frequency, so that protons located at different positions experience slightly different magnetic fields and precess at different frequencies. The slice-selection gradient determines which tissue slice is excited, the phase encoding gradient introduces spatially dependent phase shifts across the slice, and the frequency encoding (readout) gradient separates signals from different spatial locations along the readout direction. The acquired signal is sampled in k-space, which is a mathematical representation of spatial frequency and phase information. By applying a 2D inverse Fourier transform, the image is reconstructed from k-space. How the k-space is filled depends on the chosen readout method, which determines image properties such as SNR, spatial resolution, field of view, image contrast, and motion sensitivity.

2.2.4 Readout methods

The particular way in which RF pulses and magnetic field gradients are arranged in time is called an MRI pulse or imaging sequence. Two fundamental sequences are spin echo (SE) and gradient echo (GRE) sequences. SE sequences obtain contrast by using 180° RF refocusing pulses, whereas GRE sequences form the echo by rephasing the spins through reversal of the readout (frequency-encoding) gradient. The pulse sequence diagrams for SE and GRE combined with their corresponding k-space trajectory are shown in Figure 2.6 and Figure 2.7, respectively.

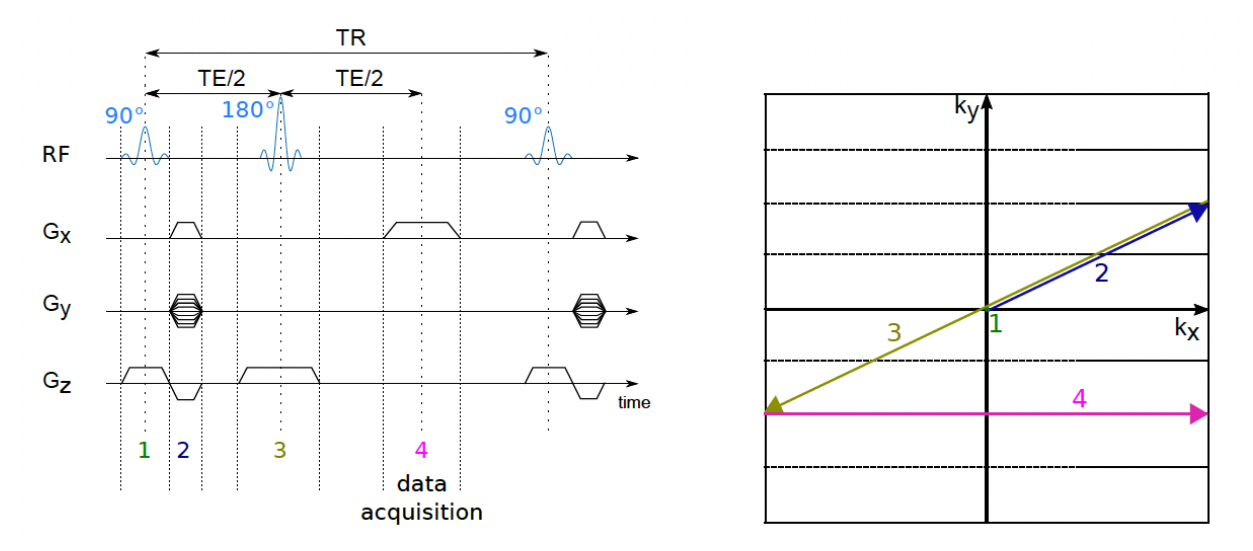


Figure 2.6: Pulse sequence of a spin echo and the corresponding k-space trajectory.

Many advanced readout methods build on these basic sequences. In this thesis, a specific GRE-based readout is used in the acquisition process: single-shot Fast Field Echo Echo Planar Imaging (FFE-EPI), with FFE referring to Philips' name for the GRE sequences.

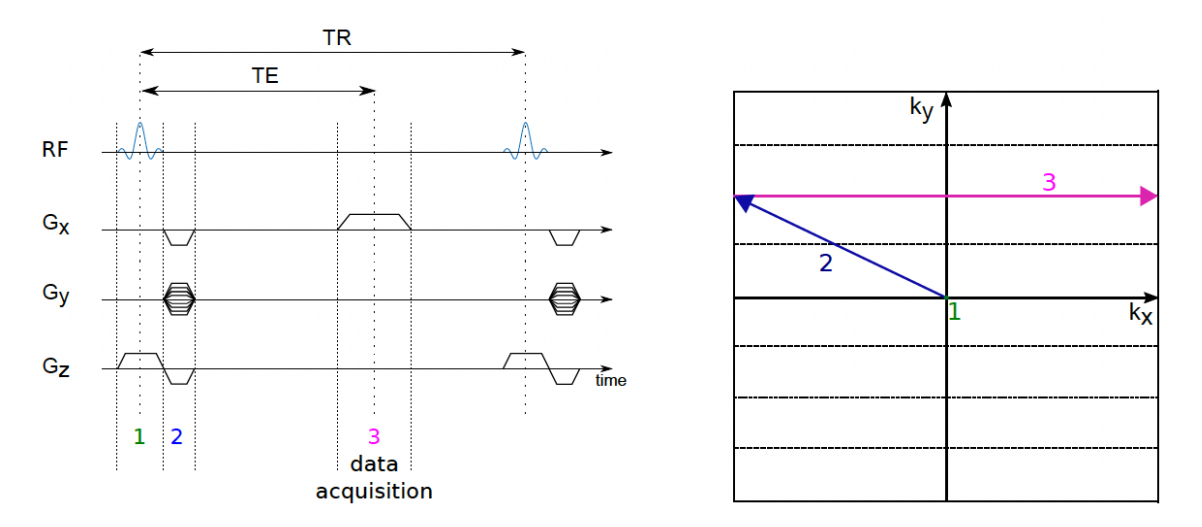


Figure 2.7: Pulse sequence of gradient echo and the corresponding k-space trajectory.

Echo planar imaging (EPI) is the fastest acquisition method in MRI, making it possible to obtain individual MR slices within 30 to 100 ms [24]. This speed reduces the effects of patient motion. Single-shot EPI means the entire two-dimensional k-space is sampled with a single RF excitation. Figure 2.8 shows a schematic of a single-shot EPI sequence.

After the excitation pulse, a combination of negative prephasing gradients in both the frequency-encoding (x) and phase-encoding (y) directions is applied. The first k-space line is then acquired during a positive readout gradient in the x-direction. Subsequently, a short positive gradient in the y-direction, referred to as a phase-enconding blip, is applied to move to the next line in k-space. The next readout occurs during a negative readout gradient in the x-direction. This alternating pattern of phase-encoding blips and oppositely directed readout gradients (train of gradient echoes) continues until all k-space lines are acquired. After the repetition time (TR), the RF excitation and gradient sequence are repeated to sample additional slices.

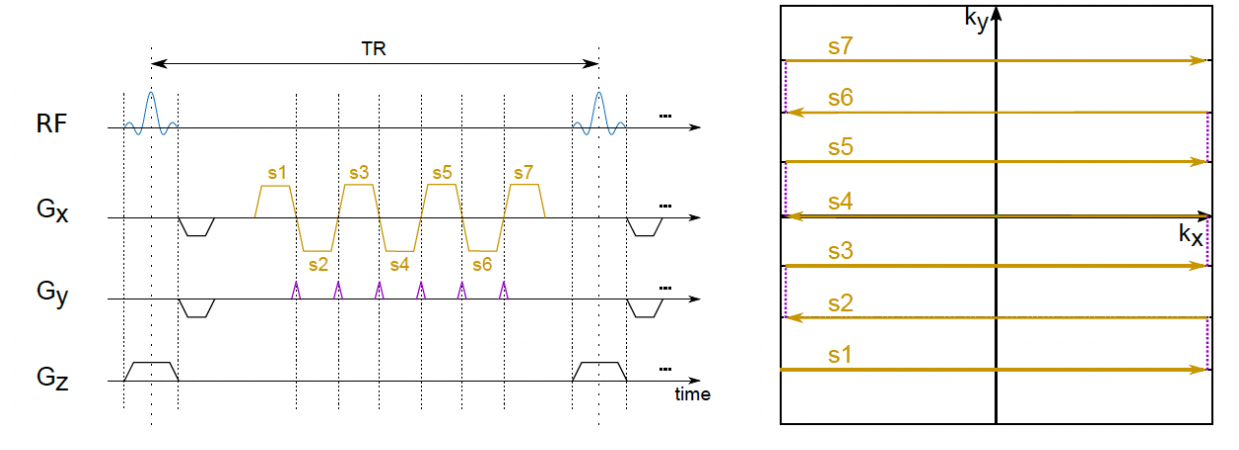


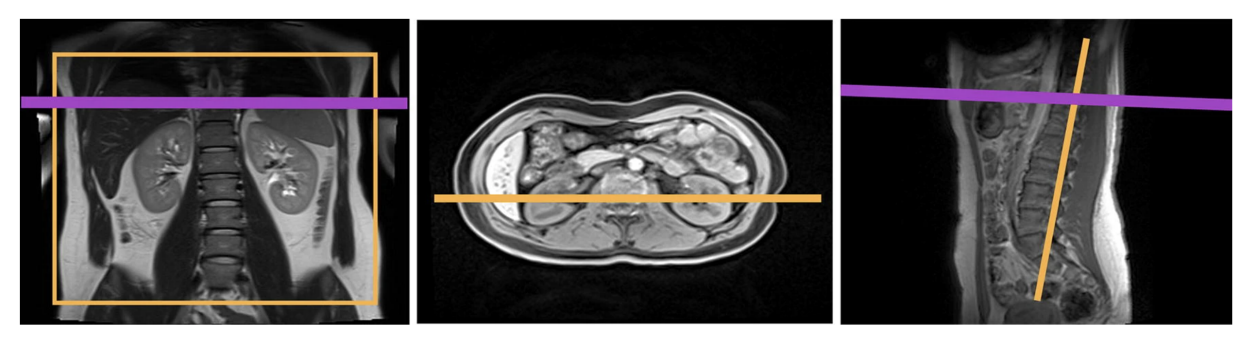
Figure 2.8: Pulse sequence of echo-planar imaging (EPI) and corresponding k-space trajectory.

2.3 Arterial Spin Labeling (ASL) MRI

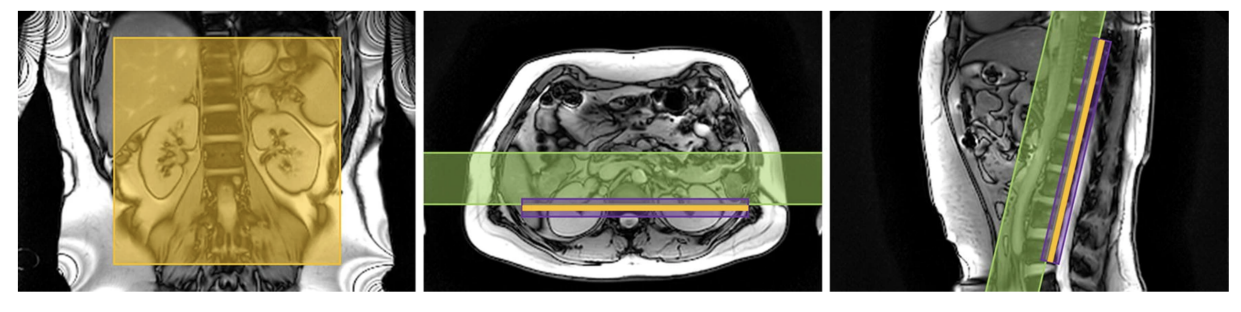
As explained in the introduction, ASL is a non-invasive MRI technique that uses magnetically labeled arterial blood water as an endogenous tracer to measure tissue perfusion. This technique quantifies perfusion by subtracting a label from a control image. The labeling image is acquired by applying a 180-degree RF pulse, also known as an inversion pulse, to invert the magnetization of blood water in the arteries before it flows into the tissue. After a post-label delay (PLD) to allow this labeled blood to enter the tissue, the label image is acquired. In the next repetition time (TR), the control image is acquired without labeling. By subtracting these two images, a unitless perfusion-weighted image (PWI) is obtained, since the only difference between them is the magnetization of inflowing blood. The differential signal is typically on the order of only a few percent of the tissue's total MRI signal. To decrease the noise and thus increase the signal-to-noise ratio (SNR), the acquisition of these label-control pairs is repeated multiple times. Furthermore, a separate calibration image (M_0) , that represents the fully relaxed magnetization of tissue water protons, is used to convert this relative signal into an absolute perfusion value during post-processing.

The two main labeling methods used in clinical practice are pseudo-continuous ASL (pCASL) and pulsed ASL (PASL). These two techniques differ in the duration of labeling and in the way the inversion of arterial blood is achieved. pCASL uses a long train of short RF pulses combined with a gradient. These short pulses label only spins flowing through a thin plane positioned upstream of the imaging region. In PASL, a short, single inversion pulse is applied over a relatively thick slab of tissue. PASL labels a large slab of arterial blood at once, which results in an unknown time duration for this labeled bolus. This bolus time varies between subjects and even across repetitions due to differences in heart rate and arterial transit time. To obtain a quantitative perfusion value using this technique, saturation pulses are added to truncate the tagged bolus using QUIPSS II or Q2TIPS. With these pulses, the bolus duration is truncated, and the amount of labeled blood contributing to the perfusion signal is constant across subjects and slices. In this thesis, arterial blood is labeled using a Pulsed Arterial Spin Labeling Flow-sensitive Alternating Inversion Recovery (PASL-FAIR) technique, which will be described in more detail below.

PASL-FAIR implements the general label—control principle described above using selective and non-selective inversion pulses. The control image is acquired with a non-selective inversion pulse that inverts the tissue and blood within the imaging slice and outside of it. For the label image, a selective inversion pulse is applied to the imaging slice. This inverts the tissue and blood spins within the imaging slice, while blood outside the slice remains uninverted. This slab should be positioned carefully to exclude the feeding arteries to avoid labeling of this blood for the selective inversion slice [20]. After a certain post-label delay (PLD), which is the time between labeling and readout, this 'fresh' unlabeled blood flows into the imaging slice. By subtracting the control from the label images, only the perfusion-related signal remains. The positioning of the inversion slab relative to the imaging slice and feeding vessels is illustrated in Figure 2.9b.



(a) Positioning of the pCASL labeling plane (purple) and imaging slice (orange) in coronal, axial, and sagittal orientations [20].



(b) Positioning of the FAIR selective inversion slab (purple), imaging slice (orange), and QUIPSSII/Q2TIPS type saturation slab (green) in coronal, axial, and sagittal orientations [20].

Figure 2.9: Positioning for pCASL and FAIR.

2.4 Mid-field MRI

The first part of the project involves data acquired at 3 T, which has already been acquired extensively [15, 25, 26, 27]. The second part explores the measurement of renal perfusion at 0.6 T, which is entirely novel. Moving from a high-field to a lower field MRI system for perfusion quantification introduces advantages and challenges, which will be discussed in this section.

2.4.1 Advantages

As explained in the introduction, advantages of low-field strengths include lower costs, improved safety, smaller footprint, and improved patient comfort. In addition, there are important technical advantages: reduced B_0 and B_1 inhomogeneities and a decreased specific absorption rate (SAR).

• Reduced B_0 inhomogeneities. Susceptibility-related artefacts such as geometric distortions are reduced because frequency shifts scale linearly with B_0 . Equation 2.1 shows that at lower B_0 , the resonance frequency decreases proportionally. This results in smaller frequency differences across tissue interfaces and leads to a reduction in off-resonance effects. This is particularly beneficial in abdominal imaging, where

air—tissue interfaces induce strong local susceptibility gradients that can otherwise lead to geometric distortions and signal loss [28].

- Increased homogeneity of B_1 field. B_1 inhomogeneities arise from the interaction of the radiofrequency (RF) field with biological tissue. This effect is less pronounced at 0.6 T because the RF wavelength is inversely proportional to the Larmor frequency, with $\lambda_{3T} \approx 0.26$ m and $\lambda_{0.6T} \approx 1.3$ m. At 3 T, the RF wavelength is of the same order as typical body dimensions, which causes electromagnetic interference patterns. These interference effects lead to spatial variations in the effective flip angle, resulting in non-uniform excitation and introducing shading artefacts. Although such effects can be prevented with certain RF pulses, such as adiabatic inversion pulses, these are not applied in the 3 T data used in this study. At 0.6 T, the RF wavelength is substantially longer than body dimensions, which suppresses the interference effects. As a result, excitation becomes more homogenous and improves the uniformity of B_1 across the field of view.
- Lower specific absorption rate (SAR). The SAR decreases with B_0 , which allows for the use of higher flip angles or longer sequences within safety limits. This means, for example, more background suppression pulses can be applied.
- Improved safety, reduced cost, and smaller footprint. Besides these technical advantages, low-field MRI systems are typically less expensive, safer than high-field systems. Moreover, they can also improve patient comfort due to reduced noise and a more open design.

2.4.2 Challenges and parameter adjustments

The fundamental challenge of using a lower field strength for ASL-MRI is the lower SNR. The magnitude of the net magnetization is directly proportional to B_0 . At a lower field strength, fewer spins align with the field than at 3 T, which results in a weaker MR signal. For an already challenging SNR method like ASL at 3 T, where the signal of interest is a small difference, this is an important concern. Additionally, the longitudinal relaxation time of arterial blood is shorter, which causes the inverted blood to return to equilibrium more rapidly, reducing the available perfusion signal by the time the blood actually reaches the tissue. To maximize SNR and capture as much perfusion signal as possible, certain sequence parameters should be adjusted for the 0.6 T ASL scans.

• Post-Labeling Delay (PLD). The PLD must be long enough to allow the tagged blood to reach the tissue, but not so long that the label has decayed. If the PLD is too short, the perfusion map may include macrovascular signal from blood that has not yet exchanged with the tissue. At 1.5 T and 3 T, a PLD of 1600 - 1800 ms is recommended. As the T_1 relaxation of blood is faster at 0.6 T, a shorter PLD compared to higher field strengths may be needed to prevent too much longitudinal relaxation. With any change in PLD, the timing of the background suppression pulses and QUIPSS II saturation pulses should also be adjusted.

- Background Suppression (BGS). Background suppression involves applying additional inversion pulses before readout to null the static tissue signal and therefore suppress physiological noise. The timing of these BGS pulses is calculated so that, at the moment of acquisition, the longitudinal magnetization of static tissue is close to zero. T_1 is shorter at 0.6 T, which means the tissue magnetization recovers faster after each inversion. For this reason, the timing of the inversion pulses should be recalculated for optimal background suppression.
- Time of Repetition (TR) and Control-Label Pairs. Due to the faster T_1 relaxation at 0.6 T, the time of repetition (TR) can be shortened. This allows for an increase in control-label pairs, while keeping the same total scan time. By increasing the number of averages, the variance of this difference signal can be reduced across repetitions because random noise will average out. Specifically, the noise level decreases with the square root of the number of repetitions (\sqrt{n}) , which improves temporal SNR (tSNR).
- In-Plane Resolution and Slice Thickness. A smaller in-plane resolution and slice thickness improves anatomical detail and minimizes partial volume effects between cortex and medulla, but at the cost of lower SNR per voxel. By using a larger voxel size without introducing too many partial volume effects, each voxel contains more spins and thus produces a higher signal.

Altogether, the PLD, BGS pulse timings, TR, the number of averages, in-plane resolution, and slice thickness can be modified and analyzed to determine the optimal acquisition settings for ASL at a lower magnetic field strength.

CHAPTER 3

Methods

This chapter is divided into two parts. The first part explains the post-processing pipeline used for the existing data acquired with a Philips 3 T MRI scanner. The second part discusses the acquisition and post-processing of new MRI data acquired at 0.6 T. The general workflow developed at the University of Heidelberg was used as a starting point for the 3 T data processing [29]. As the data used in this thesis differed from the data from Heidelberg, certain adaptations were made. The main differences between the Heidelberg workflow and the pipeline used in this work will also be highlighted.

3.1 Renal Perfusion Quantification at 3 T

The first part of this project consisted of post-processing DICOM data from the Nederlandse Epidemiologie van Obesitas 2 (NEO-2) study. This data was acquired on a Philips 3 T MRI scanner at the LUMC. Perfusion imaging was performed with a pulsed ASL flow-sensitive alternating inversion recovery (PASL-FAIR) sequence. The M_0 and ASL images were acquired with a fast field echo-planar imaging (FFE-EPI) single-shot readout. The acquisition of these MR images were single-slice coronal acquisitions with an in-plane matrix resolution of 3 x 3 mm² and a thickness of 8 mm under free breathing conditions. The M_0 scan had a long TR of 6500 ms to allow for full T_1 recovery. These images are used as a reference for quantitative perfusion calculations. The FAIR-ASL data consisted of 21 label-control pairs, with a post-labeling delay (PLD, also denoted as TI (time of inversion) for FAIR) of 1400 ms. QUIPSS-II saturation pulses were applied between 200 and 100 ms before acquisition to control the bolus duration, resulting in an effective bolus duration (TI_1) of 1200 ms. This represents the time available for blood to travel from the tagging region to the imaging region before acquisition starts (at TI = 1400 ms). Two background suppression pulses were applied at 500 ms and 1020 ms to suppress the static tissue signal. Further specifics of the ASL and M_0 parameters are listed in Table 3.1.

Parameter	ASL	M_0
Scanner	Philips 3T	Philips 3T
Sequence type	FAIR-ASL with QUIPSS-II	Proton density (M_0)
Readout sequence	FFE-EPI (single-shot)	FFE-EPI (single-shot)
Repetitions	21 label-control pairs	4
Labeling scheme	Selective inversion (SLF)	None
Label delay (TI)	1400 ms	N/A
QUIPSS-II timing	200–100 ms before acquisition	N/A
Effective bolus duration (TI ₁)	1200 ms	N/A
Background suppression	Yes (pulses at 500 & 1020 ms)	None
TR / TE	4750 ms / 17 ms	$6500 \mathrm{\ ms} \ / \ 17.7 \mathrm{\ ms}$
Flip angle	90°	90°
Voxel size	$3 \times 3 \times 8 \text{ mm}^3$	$3 \times 3 \times 8 \text{ mm}^3$
Slice orientation	Coronal	Coronal
Number of slices	1	1
Fat suppression	SPIR (strong)	SPIR (strong)
Respiratory compensation	None (free breathing)	None (free breathing)
SENSE acceleration factor	1.5 (FH)	N/A

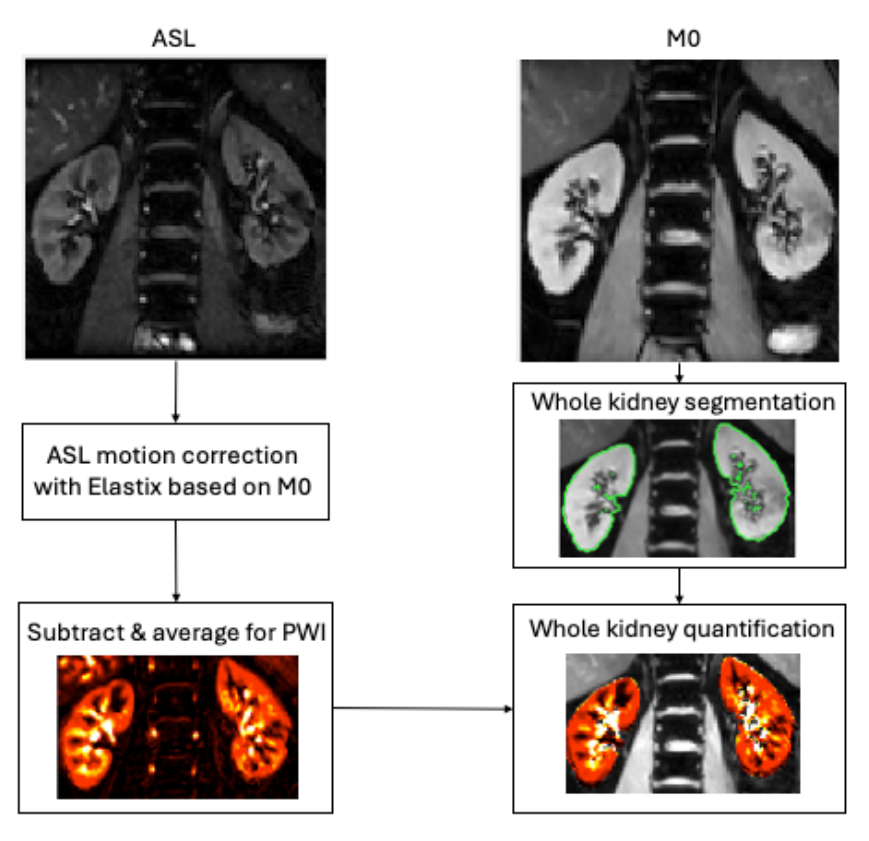
Table 3.1: FAIR-ASL and M_0 acquisition parameters for the NEO-2 study at 3 T.

These acquisition parameters were predefined at the start of this thesis. The study protocol also included a T_1 -mapping sequence using the modified Look-Locker inversion recovery (MOLLI) method. This sequence had a considerably larger FOV than the ASL and M_0 images, which made the segmentation of the cortex and medulla more complex. As data collection for the NEO-2 study was ongoing during this thesis, an updated MOLLI sequence was later added with identical FOV and geometry to the ASL and M_0 acquisitions. This breath-hold sequence provided quantitative T_1 values for each pixel in the renal cortex and medulla, along with a confidence map indicating the reliability of those the T_1 values.

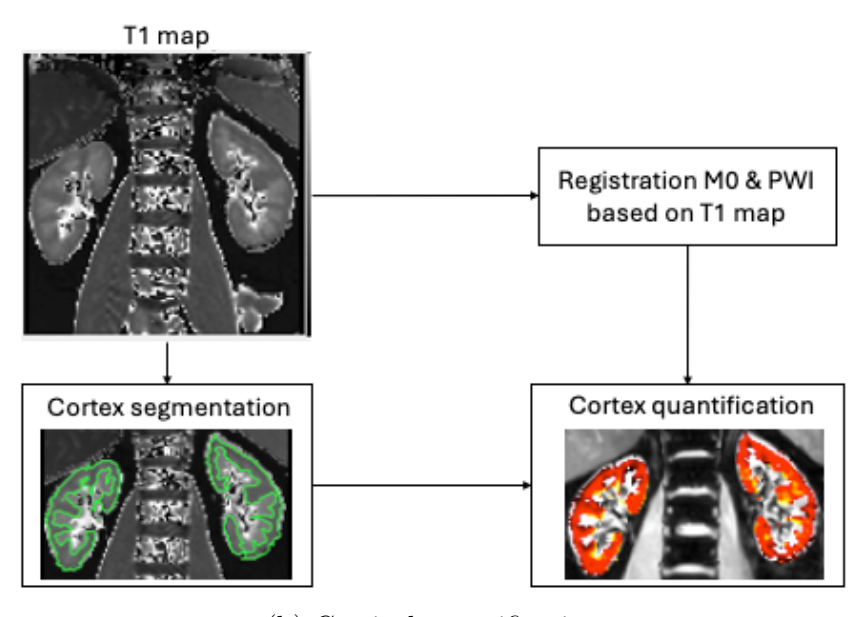
3.1.1 Analysis Pipeline for 3 T Dataset

All MRI images were imported into MATLAB from DICOM files using a loader designed to handle Philips-specific datasets. Relevant DICOM tags and protocol information were used to extract the acquisition details. All the images (ASL, M_0 , and T_1 map) were converted to numerical matrices representing the scanner signal intensities. Philips DICOM images contain per-frame scaling and rescaling factors, which were corrected in the loader to obtain the correct image intensity values. After loading the ASL, M_0 , and T_1 data as matrices, three processing steps were applied: (1) image registration, (2) segmentation, (3) perfusion quantification. An overview of these steps is shown in Figure 3.1 and described in the following sections. The final output of the analysis pipeline is a perfusion map with its corresponding cortical perfusion values. The medullary perfusion values were not analyzed in this work, as literature states the measurement of perfusion in this region is considered less reliable due to its lower perfusion and close proximity to the cortex [20]. The finalized

version of the code has been shared with Leiden University Medical Center (LUMC) and the University of Heidelberg for further refinement and validation.



(a) Whole kidney quantification.

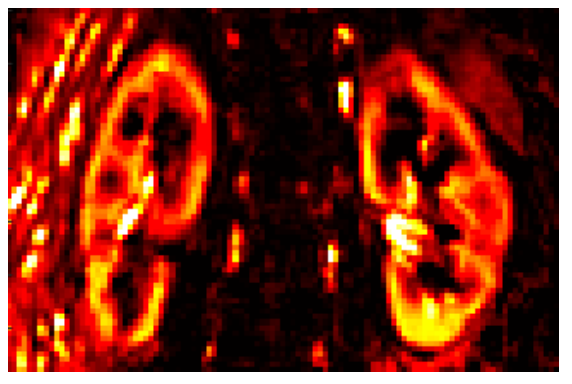


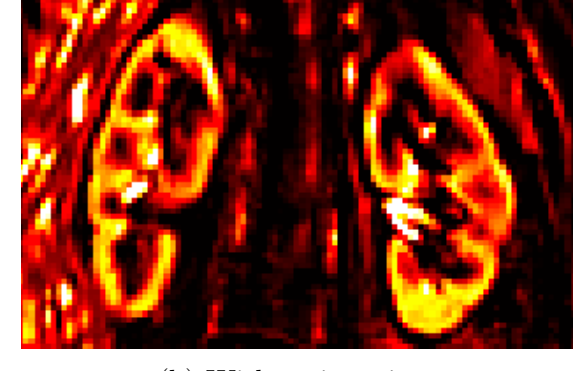
(b) Cortical quantification.

Figure 3.1: Workflow for renal perfusion quantification of (a) the whole kidney based on M_0 and (b) the cortex based on T_1 map.

3.1.1.1 Registration

The first processing step involved aligning all ASL images to correct for motion. Each control and label image was registered to an M_0 frame using the Elastix toolbox. The parameter text file provided by the University of Heidelberg was used as a baseline and was slightly adapted. The final parameter settings are provided in Appendix A. The output image type was changed from *short* to *float*, and the output format from *mhd* to *nii* to make it compatible with the Philips data. The registration result was visually checked in MATLAB and ITK-SNAP and compared to the unregistered perfusion-weighted image. In datasets without respiratory motion, registration had no effect. In cases with motion, the registration step visibly reduced blurring and sharpened the renal borders in the averaged perfusion-weighted image (Figure 3.2).





(a) Without registration.

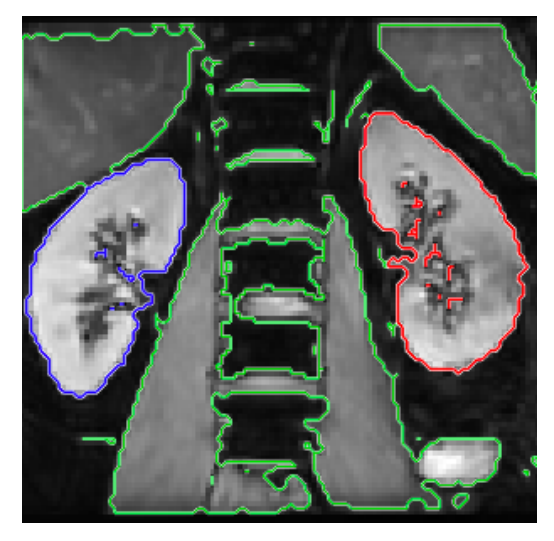
(b) With registration.

Figure 3.2: Perfusion-weighted images (a) without and (b) with registration.

3.1.1.2 Segmentation

The segmentation process was semi-automated and is illustrated in Figure 3.3. First, a histogram of the M_0 image intensities was generated to visualize the distribution of signal intensities. Based on this histogram, an intensity threshold of 30,000 (in arbitrary units) was applied to the M_0 to exclude background and non-renal tissue. Additionally, manual correction was performed to remove residual non-renal structures that were not excluded by thresholding, illustrated in Figure 3.3a.

The retrospective datasets contain the T_1 maps with a much larger field of view (FOV) than the M_0 and ASL data. Due to this mismatch in FOV, the T_1 maps could not be directly overlaid on the perfusion-weighted images, which complicated automatic cortical segmentation. To keep the processing pipeline as automated as possible, these datasets were therefore segmented based on the M_0 images, resulting in whole-kidney perfusion values. The newly acquired data included the additional T_1 maps with the same FOV and geometry as the ASL and M_0 images. This enabled automated cortical segmentation on these datasets. By analyzing T_1 values within the cortical regions of four datasets and comparing them to literature values [30], a threshold was chosen between 1200 and 1800 ms. The resulting cortical masks (Figure 3.3b) were visually verified by a radiologist.





(a) Whole kidney segmentation.

(b) Cortical segmentation.

Figure 3.3: Segmentation of (a) the whole kidney based on M_0 thresholding and manual ROI selection, and (b) the cortex based on T_1 -mapping.

3.1.1.3 Quantification

After registration, perfusion-weighted images were generated by subtracting each label image from its corresponding control image. These 21 perfusion-weighted (PWI) images were averaged to obtain a single perfusion-weighted image. The renal perfusion maps (in mL/100g/min) were then computed using:

$$f = \frac{6000 \cdot \lambda \cdot \text{PWI}_{\text{avg}} \cdot e^{\frac{TI}{T_{1b}}}}{2 \cdot \alpha \cdot TI_1 \cdot M_0},$$
(3.1)

where λ is the blood–tissue partition coefficient (0.9), TI is the inversion time or postlabeling delay (1.40 s), T_{1b} is the longitudinal relaxation time of blood (1.65 s), α is the labeling efficiency including background suppression (0.95 × 0.93^{nbs}), and TI_1 is the effective bolus duration (1.20 s). For this dataset, two background suppression pulses ($n_{BS} = 2$) were applied (see Table 3.1). This equation is the standard ASL equation for pulsed labeling with QUIPSS-II, recommended in the consensus guidelines for renal ASL [20]. It was applied per pixel to generate a perfusion map. Subsequently, by using the kidney masks defined during segmentation, cortical perfusion values were extracted.

3.1.2 Heidelberg 2020 vs. Current Pipeline

The workflow from the University of Heidelberg (2020) was used as a foundation. Since this code did not include cortical segmentation with T_1 maps, some steps were adjusted and added. The key differences between the two pipelines are summarized in Table 3.2.

Heidelberg (2020) Current Pipeline Aspect Control/label $\rightarrow M_0$ (i) Control/label $\rightarrow M_0$, (ii) Registration Derived PWI + $M_0 \rightarrow T_1$ mapa M_0 as fixed for ASL (i) M_0 as fixed for ASL, (ii) Reference image T_1 map as fixed for derived PWI and M_0 (i) Thresholded using M_0 , Whole-kidney segmentation Manual ROIs on M_0 (ii) Manual clean-up^b Thresholded using T_1 map Cortex segmentation Not implemented^c

Table 3.2: Differences between the Heidelberg pipeline from 2020 and the current pipeline.

3.2 Renal Perfusion Quantification at 0.6 T

The second part of the project focused on acquiring new data using a Philips 0.6 T scanner and post-processing this data using a slightly adapted pipeline.

3.2.1 Acquisition

Thickness

Post Label Delay (PLD)

Background suppression

As explained in Chapter 2, several sequence parameters need to be adjusted at a lower field strength to compensate for differences in relaxation and SNR. The 3 T scan protocol was used as a baseline, and specific parameters were modified for the 0.6 T acquisition (Table 3.3). These modifications are based on the theoretical background and the consensus paper [20]. The justifications for these choices are explained in the following sections.

Parameter	3 Tesla	0.6 Tesla
Repetitions	21 control-label pairs	Up to 30 control-label pairs
Time of Repetition (TR)	4750 ms	3500 & 4000 ms
In-plane resolution	$3 \times 3 \text{ mm}^2$	$3 imes 3 ext{ mm}^2 \& 4 imes 4 ext{ mm}^2$

Yes (500 & 1020 ms)

8 mm

 $1400 \; \mathrm{ms}$

Table 3.3: FAIR-ASL parameters changed for the 0.6 T MRI scanner

Two BGS timing schemes were tested at 0.6 T (see text): a timing of 700 & 1100 ms (with QUIPSS-II at 200 & 100 ms) and a timing of 670 & 1150 ms (with QUIPSS-II at 100 & 50 ms).

8 mm & 10 mm

1200, 1400, & 1800 ms

Yes (700, 1100) & (670, 1150)

^a This additional registration step is performed only for datasets where a matching FOV T_1 map is available

^b Manual cleanup to remove surrounding tissues with similar intensity values.

^c The Work In Progress (WIP) follow-up code from the University of Heidelberg was reviewed. This code does segment the cortex (and medulla) using perfusion-based clustering. However, this introduces a dependent variable as perfusion values may be abnormal for patients.

3.2.1.1 Control-Label Pairs and Repetition Time (TR)

The consensus recommendations suggest acquiring at least 20 control-label pairs [20]. In this study, the number of pairs was increased to 30 to partially compensate for the lower SNR expected at 0.6 T. The temporal SNR (tSNR) of the averaged perfusion image is theoretically expected to improve with the square root of the number of repetitions (\sqrt{n}). To assess the practical improvement in tSNR, the cortical tSNR across 20, 25, and 30 pairs is compared by drawing an ROI on the perfusion-weighted image. However, increasing this number also increases the acquisition time, since each additional label–control pair adds two TR periods. The NEO-2 study uses a TR of 4750 ms and 21 label-control pairs, which takes approximately 3 minutes and 20 seconds. As 0.6 T gives a faster T_1 decay, theoretically, allowing the TR to be shortened. It should be taken into account that a too short TR results in less recovery and thus a weaker signal. Two TRs, 4000 ms and 3500 ms, were evaluated using 30 label–control pairs, corresponding to total acquisition times of 4 minutes and 3 minutes 30 seconds, respectively.

3.2.1.2 In-Plane Resolution and Slice Thickness

The same consensus paper mentions choosing an in-plane resolution with a maximum of $4 \times 4 \text{ mm}^2$ and a thickness of 8 mm for renal ASL. For this study, in-plane resolutions of $3 \times 3 \text{ mm}^2$ (same as the 3 T protocol) and $4 \times 4 \text{ mm}^2$ were tested. A larger in-plane resolution is expected to provide higher SNR, at the expense of reduced spatial detail. Regarding the slice thickness, a length of 10 mm was chosen to compare to 8 mm. Although 10 mm is more than the consensus paper advises, the thickness of the kidneys is approximately 47 mm [31]. After consultation with a radiologist and verification on CT images, this increase in thickness was deemed acceptable as the most important aim is to increase signal. Increasing slice thickness improves SNR, but may also introduce partial volume effects. By only increasing this thickness by 4% compared to the kidney thickness, this effect is minimized.

3.2.1.3 PLD and BGS pulses

At a lower field strength, T_1 values are shorter. Consensus recommendations for renal ASL acquisitions at 1.5 T and 3 T suggest PLDs in the range of 1600–1800 ms, while the NEO-2 study at 3 T used a PLD of 1400 ms. To evaluate which PLD should be used for 0.6 T, three PLDs were tested: 1200 ms, 1400 ms, and 1800 ms. As the PLD changes, the timing of the BGS pulses should also be adjusted accordingly. The optimal BGS timings were determined using a MATLAB-based simulation. The goal of these simulations was to minimize the longitudinal magnetization (Mz) of background tissues at the start of readout to maximize static tissue suppression. If the BGS drives M_z too close to zero, small variations in T_1 or BGS efficiency can cause M_z to become negative. This would introduce subtraction artifacts. To avoid this, the residual M_z of background tissue should remain slightly positive, in the order of 10-20%. In the MATLAB simulation for a PLD of 1400 ms, the optimal BGS pulse times were at 670 and 1200 ms. However, to avoid M_0 crossing zero and thus prevent the subtraction artefacts, 700 and 1100 ms are taken as a baseline.

3.2.2 Analysis Pipeline 0.6 T

The post-processing pipeline for the 0.6 T data was based on the 3 T pipeline described in Section 3.1, with minor adjustments for low-field parameters. The same image registration and segmentation procedures were applied. The perfusion quantification used the same formula as at 3 T, but with an adjusted value for T_{1b} of 1.122 s, which was retrieved from an article evaluating this value at 0.55 T [32]. The PLD (or TI) and bolus duration (TI_1) values in the equation were set according to the chosen 0.6 T ASL protocol (as determined by the acquisition optimization results).

To assess whether the 0.6 T scanner can be used to reliably quantify renal perfusion, a comparison was performed with 3 T as a reference. A healthy volunteer was scanned consecutively on the same day at 3 T and 0.6 T, with identical positioning. The resulting perfusion maps and cortical perfusion values from the two field strengths were compared to assess the agreement and differences.

CHAPTER 4

Results

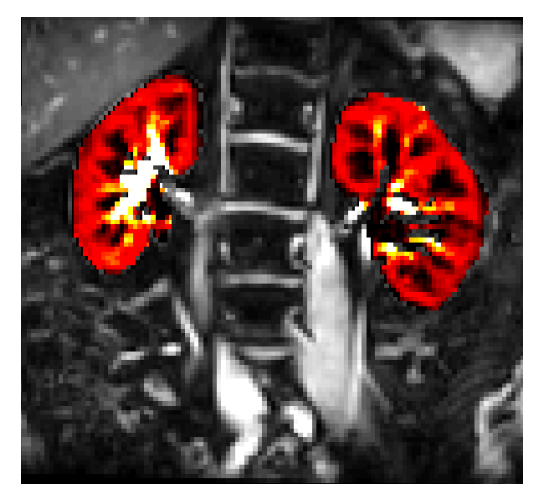
This section consists of four main parts. First, the results from the 3 T acquisitions of the NEO-2 study are presented. This includes cortical perfusion values from multiple patients and the perfusion map of one of these subjects. Second, the results of the 0.6 T acquisition parameter tests are presented. The effects of modifying several parameters are evaluated through quantitative tSNR analysis and visual analysis of the perfusion-weighted images. Based on these findings, the optimal parameters are identified. The third part of this chapter focuses on post-processing the mid-field MRI data with the adjusted pipeline. Finally, perfusion maps and the corresponding cortical perfusion values are compared at 0.6 T and 3 T for the same subject.

4.1 Renal Perfusion Results at 3 T

A renal perfusion map obtained from the NEO-2 study, along with the segmented cortical perfusion map, is shown in Figure 4.1. Table 4.1 summarizes the mean cortical perfusion values (with standard deviations, SD) for both kidneys measured in four patients from the NEO-2 study, including Patient 1. Cortical perfusion values in these subjects range from 183 to 265 mL/100 g/min.

Table 4.1: Mean cortical perfusion values (\pm SD) in mL/100g/min for all four patients.

Patient	Left cortex	Right cortex
Patient 1	200.91 ± 76.65	231.65 ± 134.15
Patient 2	265.54 ± 127.25	244.85 ± 167.37
Patient 3	183.62 ± 112.72	190.21 ± 102.16
Patient 4	220.46 ± 113.61	219.83 ± 75.85



(a) Whole kidney perfusion map



(b) Cortical perfusion map

Figure 4.1: Renal perfusion maps for patient 1 of (a) the whole kidney and (b) the cortex.

4.2 Renal Perfusion Results at 0.6 T

This part of the project includes the acquisition and post-processing results. As explained in the methods section, the influence of certain parameters was analyzed. As a baseline, an in-plane resolution of 4×4 mm², a slice thickness of 8 mm, a repetition time (TR) of 4000 ms, and 30 control-label pairs were used. The PLD was kept at 1400 ms, but the background suppression pulses were applied at 700 and 1100 ms. Figure 4.2 shows the M_0 image and the first control and label images acquired with these baseline settings. Using this baseline as a reference, the effect of changing the number of pairs, TR, voxel size, PLD, BGS timing, and readout sequence is evaluated and detailed below.

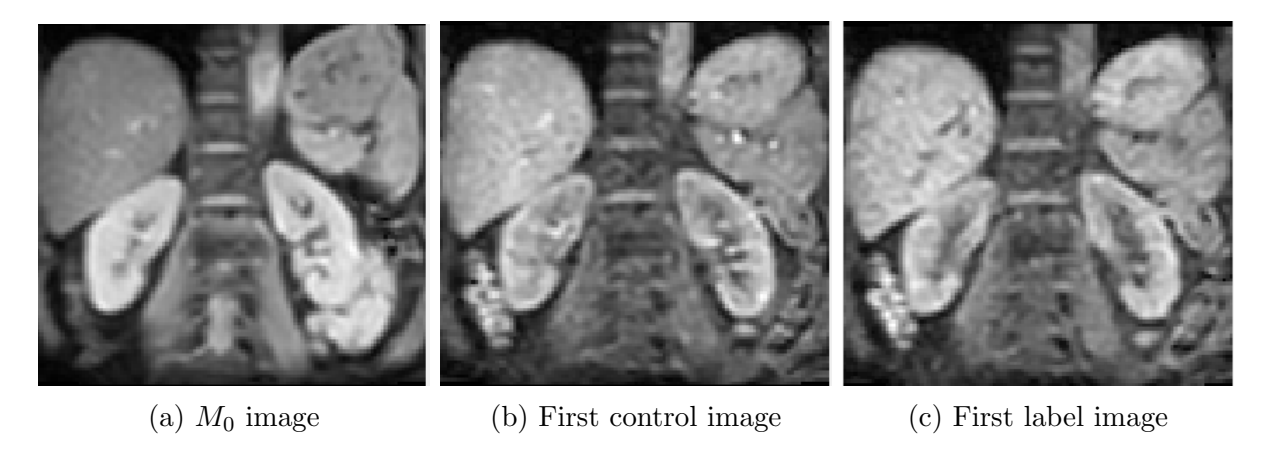


Figure 4.2: First MR images acquired at 0.6 T: (a) M_0 image, (b) first control image, and (c) first label image.

4.2.1 Repetition Time (TR) and Control-Label Pairs

In Figure 4.3, the perfusion-weighted images (PWIs) are shown for 20, 25, and 30 control—label pairs at repetition times (TR) of 3500 and 4000 ms. The manual segmentation of the left cortex used for the tSNR analysis is shown in Figure 4.4.

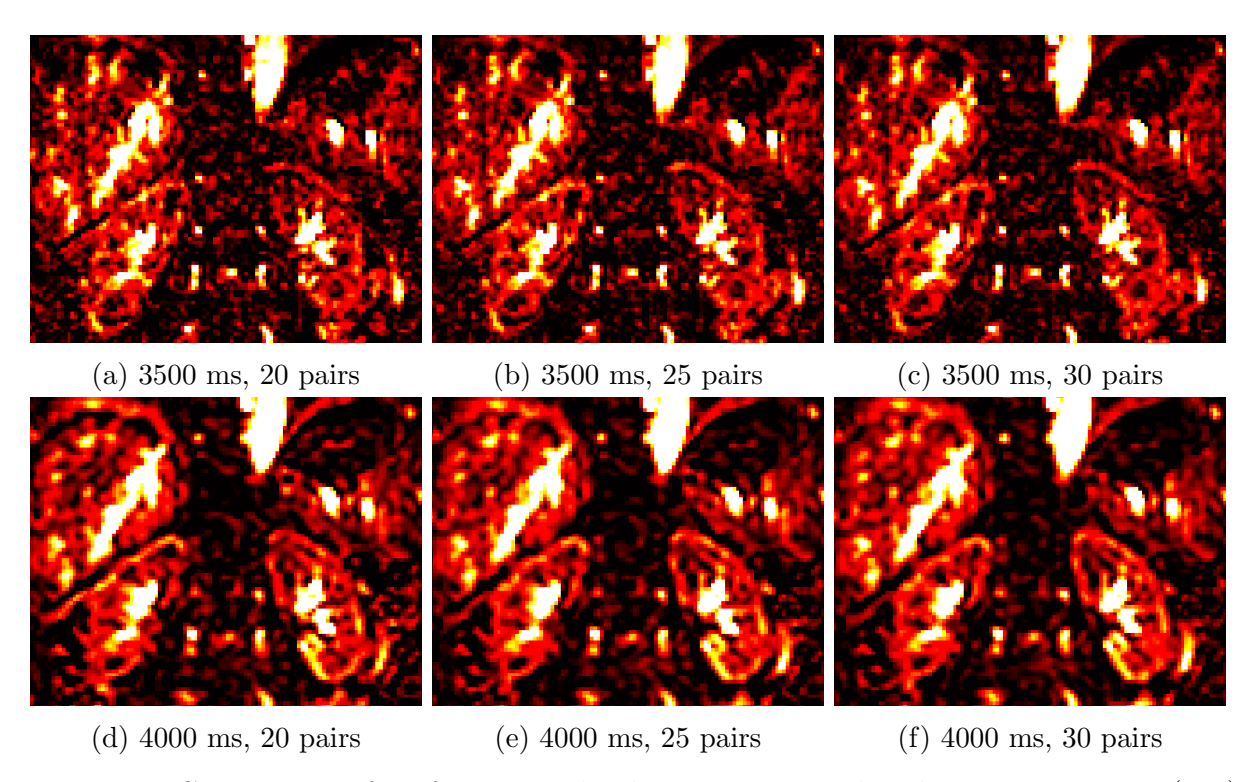


Figure 4.3: Comparison of perfusion-weighted images acquired with repetition times (TR) of 3500 ms (top row [a, b, c]) and 4000 ms (bottom row [d, e, f]) using 20, 25, and 30 control—label pairs.

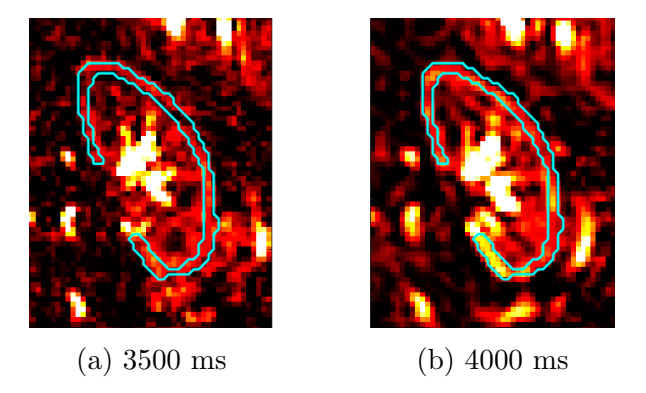


Figure 4.4: Manual cortical segmentation based on perfusion-weighted images (PWI) acquired with 30 control—label pairs at repetition times (TR) of (a) 3500 ms and (b) 4000 ms.

The influence of the number of control pairs and length of TR on the quality of the PWI for the left kidney is illustrated in Figure 4.5. Increasing the TR from 3500 to 4000

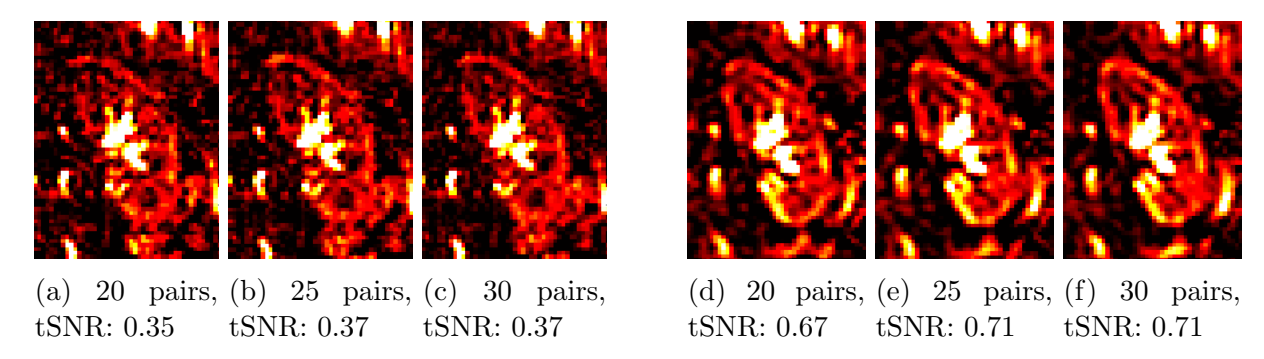


Figure 4.5: Perfusion-weighted images of the left kidney acquired with repetition times (TR) of 3500 ms (left side [a, b, c]) and 4000 ms (right side [d, e, f]) for 20, 25, and 30 control—label pairs with corresponding cortical tSNR values.

ms gives a visually smoother image with a clearer delineation of kidney borders and renal cortex. This qualitative improvement is supported by quantitative analysis: the cortical tSNR values increase from 0.37 at TR=3500 ms to 0.68 at TR=4000 ms for 30 controllabel pairs. Furthermore, increasing the number of controllabel pairs also improves tSNR, but this effect plateaus at a higher number of pairs. At a TR of 3500 ms, cortical tSNR remains nearly constant between 25 and 30 pairs. Similarly, at a TR of 4000 ms, this tSNR also plateaus after 25 pairs.

4.2.2 In-Plane Resolution and Slice Thickness

In-Plane Resolution. Figure 4.6 and Figure 4.7 show the difference between in-plane resolutions of $4 \times 4 \text{ mm}^2$ and a $3 \times 3 \text{ mm}^2$. The larger in-plane resolution, $4 \times 4 \text{ mm}^2$, gives a much clearer outline of the kidney and distinction between cortex and medulla. This is also supported by the tSNR value for the two different resolutions, which increases from 0.44 to 0.72 for the left cortex.

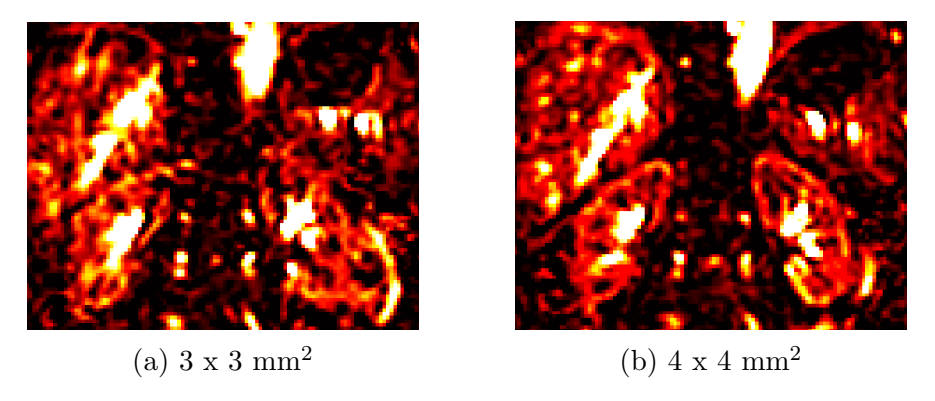


Figure 4.6: Comparison of in-plane resolutions for the perfusion-weighted images: (a) $3 \times 3 \text{ mm}^2$ and (b) $4 \times 4 \text{ mm}^2$.

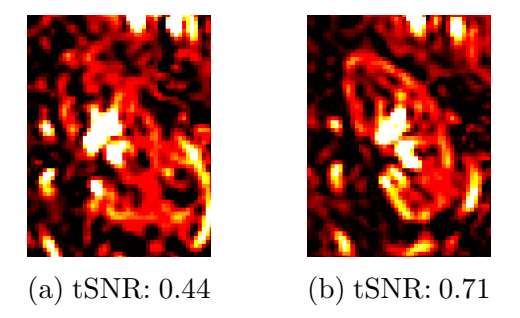


Figure 4.7: Perfusion-weighted images of the left kidney for two in-plane resolutions: (a) $3 \times 3 \text{ mm}^2$ and (b) $4 \times 4 \text{ mm}^2$.

Slice Thickness. Figure 4.8 shows the effect of an increase in slice thickness from 8 mm to 10 mm. As expected, the thicker slice produces a higher overall signal intensity as can be observed by the increased image brightness. The tSNR also increases along with the thickness, with a left cortical tSNR of 0.71 for 8 mm and 0.75 for 10 mm. The larger slice shows motion artifacts, which complicates comparison before post-processing.

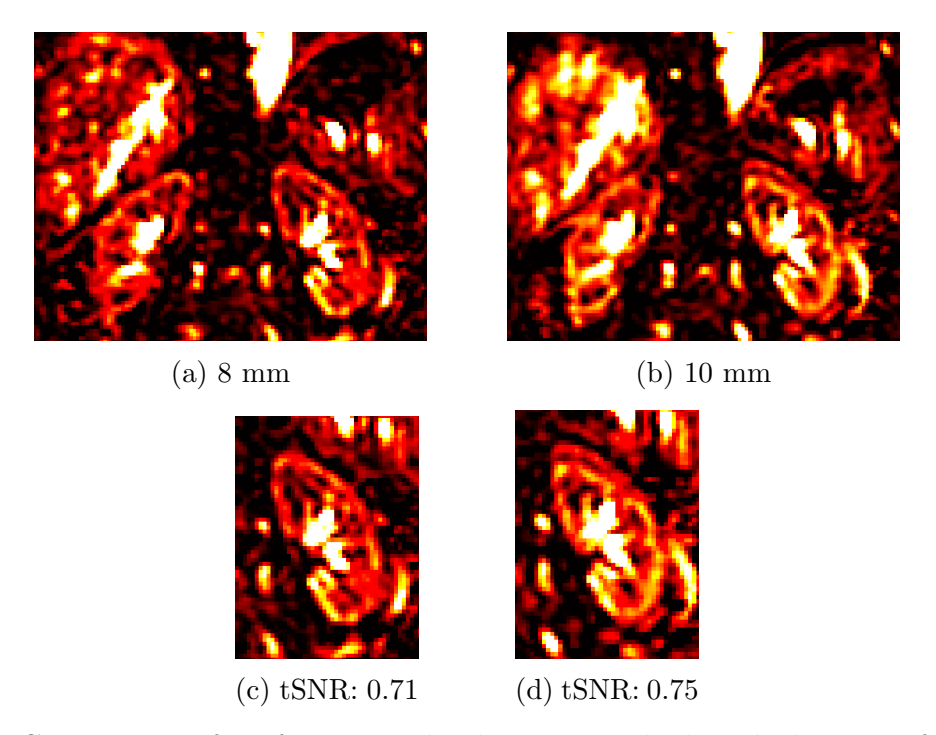


Figure 4.8: Comparison of perfusion-weighted images with slice thicknesses of 8 mm and 10 mm. Full-field images are shown in (a) and (b), and the cropped versions visualizing the left kidney images are shown in (c) and (d) with their corresponding cortical tSNR values.

4.2.3 Post Label Delay (PLD)

In Figure 4.9, the PLDs of 1200, 1400, and 1800 ms are compared along with their corresponding calculated optimal BGS pulse timings. At a PLD of 1200 ms, the PWI shows a strong macrovascular signal in the pelvis region. Increasing the PLD to 1400 ms shows a clearer perfusion-weighted contrast between cortex and medulla and a clearer kidney outline. With a PLD of 1800 ms, the overall signal intensity is decreased.

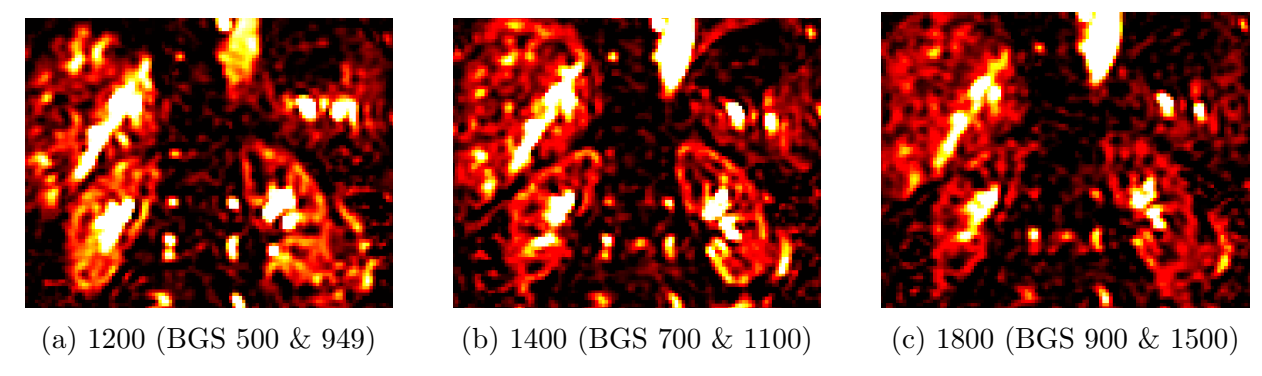


Figure 4.9: Comparison of perfusion-weighted images with post-labeling delays (PLD) and background suppression (BGS) pulse timings: (a) PLD = 1200 ms, (b) PLD = 1400 ms, and (c) PLD = 1800 ms.

4.2.4 Background Suppression (BGS) pulses

To evaluate the influence of BGS, two timing schemes were compared at with PLD of 1400 ms, TR of 4000 ms, and a voxel size of $4 \times 4 \times 10 \text{ mm}^3$.

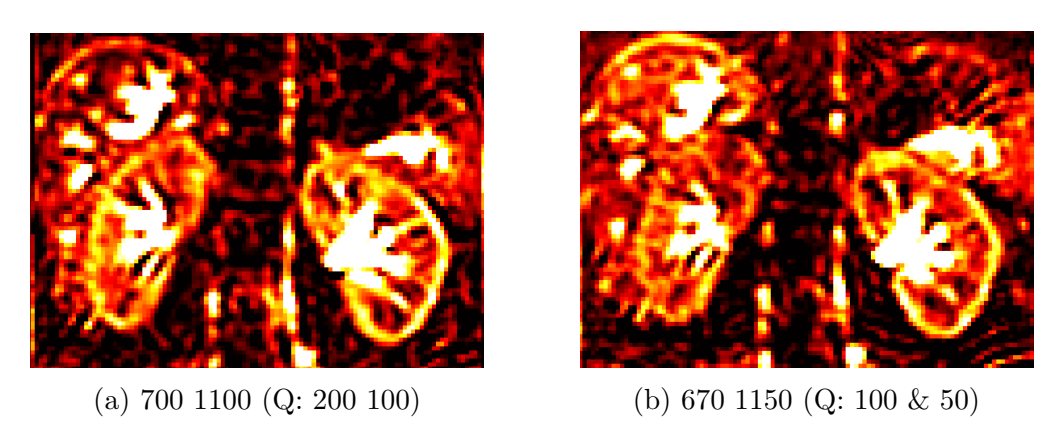


Figure 4.10: Comparison of perfusion-weighted images acquired with different background suppression (BGS) pulse timings: (a) 700 & 1100 ms and (b) 670 & 1150 ms. Whole image tSNR values were 0.48 and 0.41, respectively.

Figure 4.10 shows the BGS timings of 700 and 1100 ms (with QUIPSSII timings at 200 and 100 ms), compared with the BGS timing of 670 and 1150 ms (with QUIPSS at 100 and 50 ms). This figure shows the motion-corrected perfusion-weighted images, as the unprocessed images contained movement. This results in a more reliable analysis. The

700/1100 timing resulted in a more effective suppression of background tissue signal, which is mainly visible in the right kidney (see Figure 4.10a). The 670/1150 timing appears to have slightly less effective suppression, and the outline of the right kidney fades into the background. The tSNR of the whole image is higher for 700/1100 with 0.48 compared to 670/1150 with 0.41.

4.2.5 Post-processing

Based on the acquired PWIs, the following parameters were chosen as the optimal 0.6 T ASL protocol: PLD of 1400 ms, BGS pulses at of 700 and 1100 ms with QUIPSS II saturations at 200 ms and 100 ms before readout, a TR of 4000 ms, 25 control-label pairs, and an in-plane resolution of 4×4 mm² with a slice thickness of 10 mm.

4.2.5.1 Registration

The same registration method was applied to the 0.6 T data as was used for the 3 T dataset. The effect of registration is illustrated in Figure 4.11. After registration, there is a clearer delineation of the kidney boundaries and between the cortex and medulla. This confirms that the registration step is effective in reducing motion artifacts in the 0.6 T data as well.

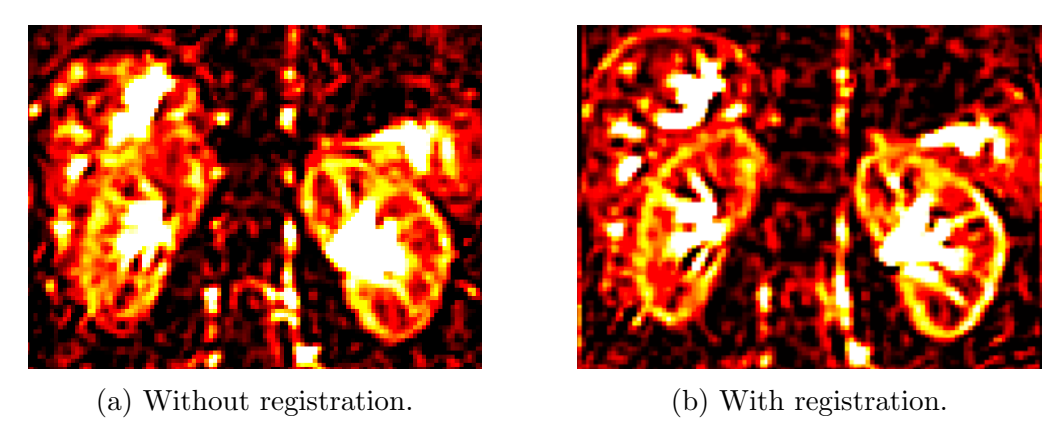


Figure 4.11: Effect of image registration on perfusion-weighted images: (a) without registration and (b) after registration.

4.2.5.2 Segmentation

At 0.6 T, only whole-kidney masks could be generated due to the absence of a correctly acquired T_1 MOLLI sequence. The whole kidney segmentation was obtained using the same approach as for the retrospective NEO-2 data: applying a threshold to the M_0 image and manually correcting the region of interest (ROI). Figure 4.12 shows an example of an erroneous T_1 map, where anatomically correct contrast between the cortex and medulla was not obtained.

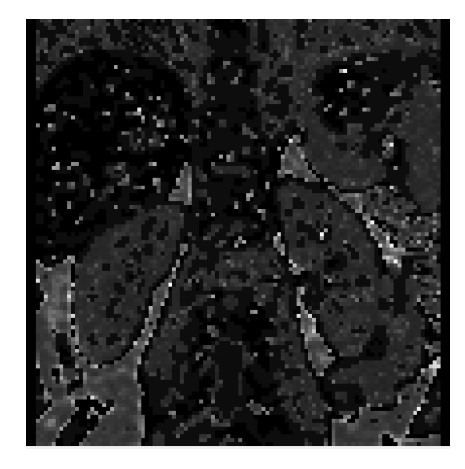


Figure 4.12: Example of an erroneous T_1 map acquired at 0.6 T.

4.3 Comparison of Renal Perfusion at 3 T and 0.6 T

The M_0 image and first control-label pair for the same person acquired at 3 T and 0.6 T are shown in Figure 4.14 and 4.13, respectively. The main visual differences between the two field strengths are the SNR, tissue contrast, and EPI-related artefacts.

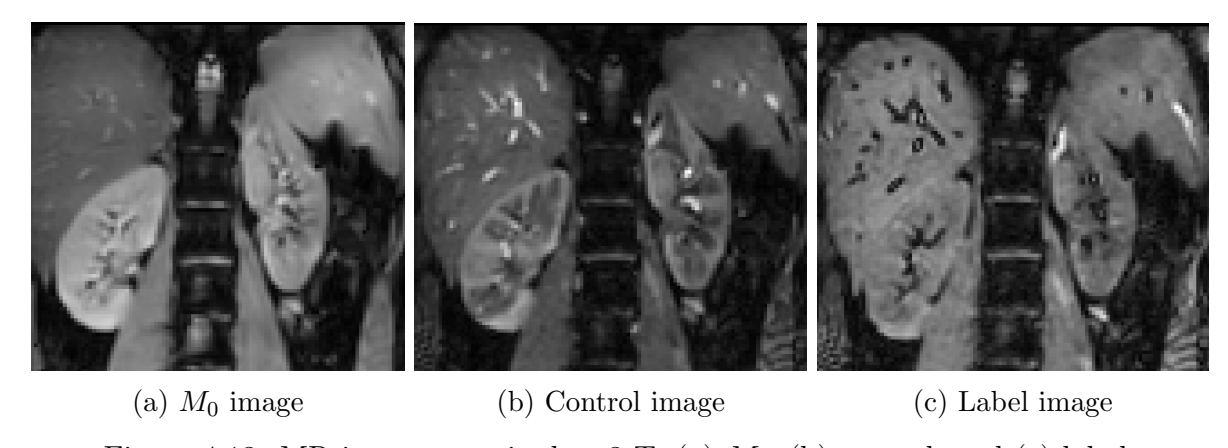


Figure 4.13: MR images acquired at 3 T: (a) M_0 , (b) control, and (c) label.

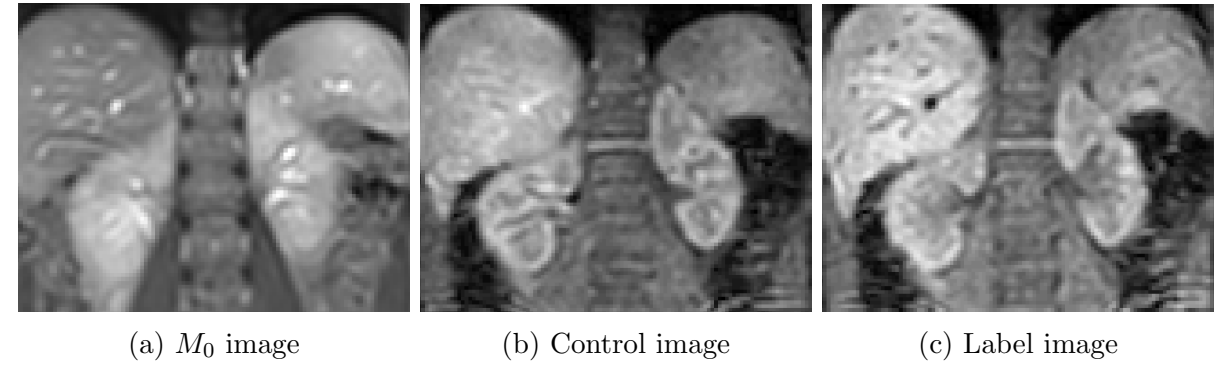


Figure 4.14: MR images acquired at 0.6 T: (a) M_0 , (b) control, and (c) label.

Firstly, a much lower SNR is observed at the lower field strength. This observation is qualitatively confirmed by the non-registered tSNR maps of the averaged perfusion weighted images, which are shown in Figure 4.15. Based on these maps, the cortical tSNR of the left kidney was derived by drawing a manual ROI. This resulted in a tSNR of 2.2406 at 3 T, more than three times higher than the 0.7202 measured at 0.6 T. In addition to the lower tSNR, the maps also reveal a more homogeneous spatial signal distribution for the kidney at 3 T, particularly for the right kidney.

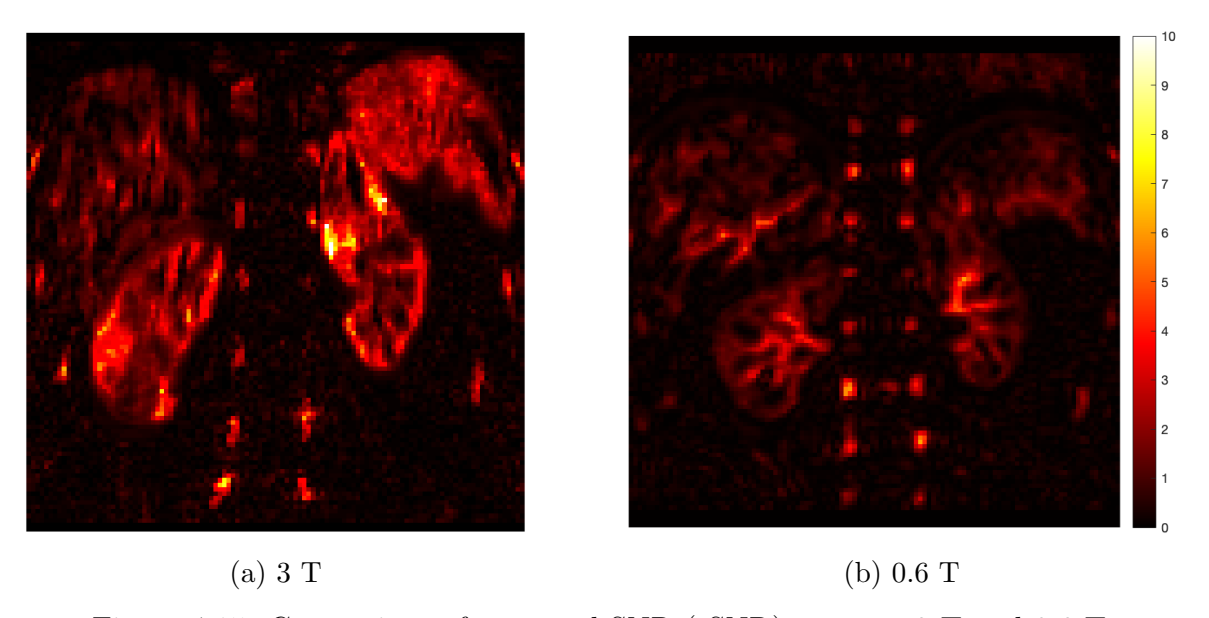


Figure 4.15: Comparison of temporal SNR (tSNR) maps at 3 T and 0.6 T.

Secondly, the 3 T images show geometric distortion caused by magnetic field inhomogeneities. This is visible as a stretching of the kidney shape in the phase-encoding direction and as a distortion of the liver. The two field strengths also differ in tissue contrast, with the higher field showing more contrast between certain tissues. The whole-kidney and cortical perfusion maps at 3 T and 0.6 T are shown in Figure 4.16 with the corresponding cortical perfusion values listed in Table 4.2. The mean cortical perfusion was approximately 5-10% higher at 3 T compared to 0.6 T for both the left and right cortex.

Table 4.2: Mean cortical perfusion values for left and right kidney cortex at 3 T and 0.6 T. Values are given in mL/100g/min (mean \pm SD).

	Left cortex	Right cortex
3 T	241.89 ± 76.55	250.75 ± 70.82
$0.6~\mathrm{T}$	215.34 ± 67.92	236.80 ± 66.33

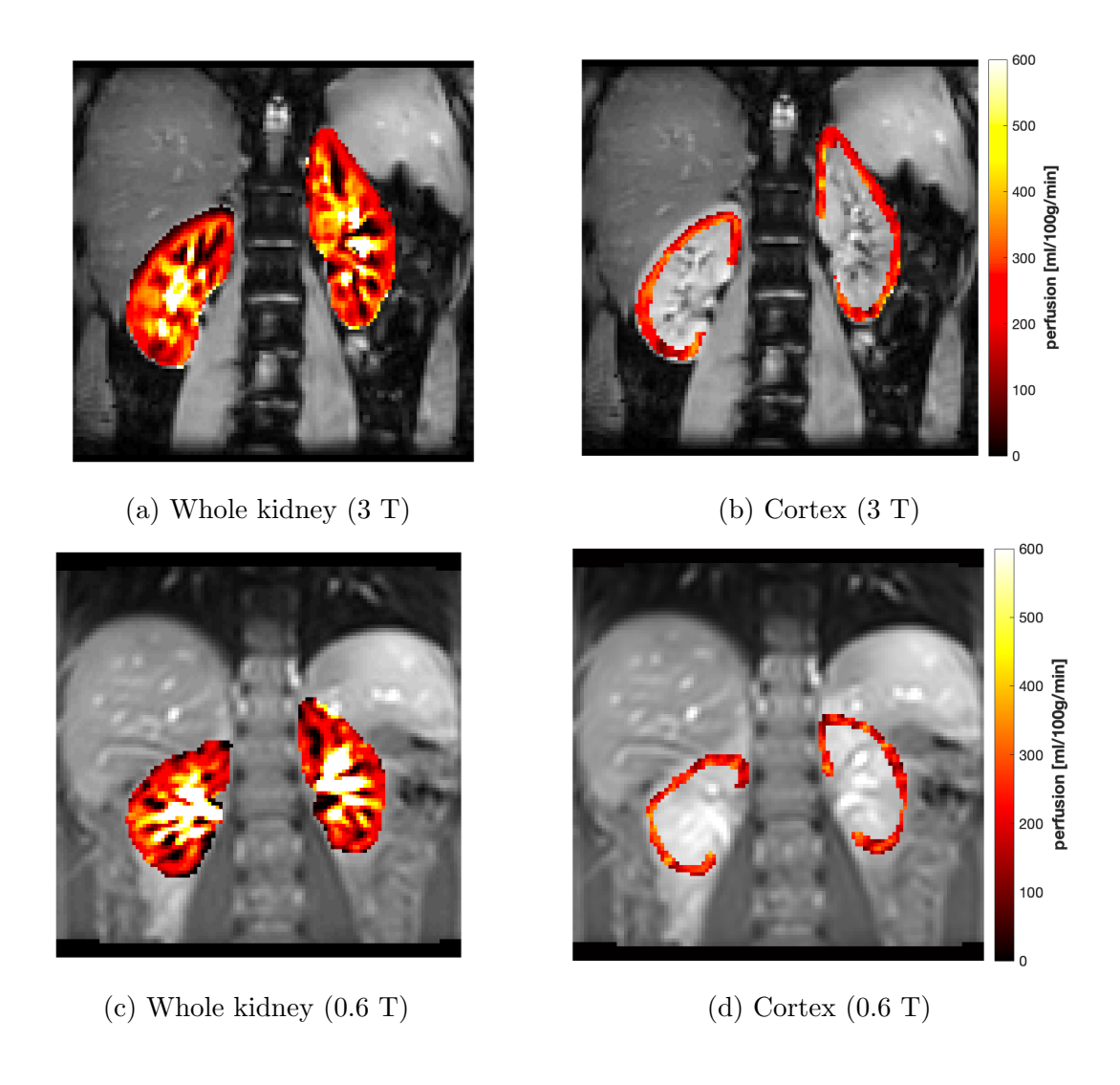


Figure 4.16: Whole kidney and cortical perfusion maps at 3 T (top row) and 0.6 T (bottom row).

Chapter 5

Discussion

This chapter discusses the results obtained in this thesis. First, the renal ASL analysis pipeline at 3 T and the corresponding perfusion values are discussed. Second, the effects of different acquisition parameters at 0.6 T are interpreted. Lastly, the results from 3 T and 0.6 T are compared to evaluate the feasibility of renal perfusion quantification at this mid-field strength.

5.1 Renal Perfusion Results at 3 T

The cortical perfusion values ranged from 183 mL/100g/min to 265 mL/100g/min for the four analyzed cases from the NEO-2 study obtained at 3 T. These values are consistent with the reported physiological range in literature. A systematic review on ASL-based renal perfusion values showed a range of cortical blood flow measures measured between 139 and 427 mL/100g/min in healthy volunteers and from 83 to 412 mL/100g/min in a broad range of patient groups [33]. However, the measured standard deviations of these values are relatively high, in some cases nearly up to 50% of the mean cortical perfusion. Such a large variation suggests heterogeneity of the perfusion maps. This can be a result of several factors, such as physiological fluctuations, scanner settings, or post-processing inaccuracies.

This quantitatively high standard deviation can be observed within the perfusion maps. Spatial variation could be explained by regional differences linked to local autoregulatory mechanisms. However, the perfusion map mainly shows small hotspots around the renal pelvis region. These hotspots are visible before image registration and become more pronounced after the ASL subtraction and perfusion quantification steps. Given this visibility before post-processing and the fact that the renal pelvis contains urine and adjacent vasculature, the hotspots are likely a result of physiological signal or scanner settings (pa-

rameters, positioning) rather than artifacts introduced by the post-processing workflow. For instance, the dataset uses a PLD of 1400 ms, whereas the renal consensus paper recommends a minimum of 1600 ms. This shorter PLD could lead to macrovascular artefacts if the labeled blood has not yet fully exchanged into the tissue by the time of image readout.

As this thesis was conducted within a limited time frame, a choice was made to produce a functioning workflow without fully optimizing every processing step. The motion correction step that registered the ASL images to M_0 produced satisfactory results. However, to segment the cortex automatically, the PWI and M_0 are registered to the T_1 map. The ASL and M_0 images are both acquired with an FFE-EPI readout, which introduces susceptibility artefacts, whereas the T_1 map does not. This second registration step introduces more misalignment due to differences between distorted (EPI) and undistorted (T_1 -mapping) images. As a result, voxels in the cortical mask may not perfectly correspond to the same anatomical regions in the ASL data, mixing signals from cortex, medulla, or surrounding tissue. This partial-volume mixing increases the variability in measured cortical perfusion, which may also explain the relatively large standard deviations observed. Therefore, future research could aim to reduce this source of error by adjusting the parameter text file or incorporating multiple registration stages.

Second, segmentation of the cortex was performed using manually selected intensity ranges from the T_1 map histogram. Although these ranges successfully segmented the cortex for the analyzed datasets, this approach is sensitive to inter-patient variability and to differences in T_1 scaling across scanners or field strengths. For example, a fixed T_1 range might misclassify the cortical tissue if a patient has a typically high cortical T_1 value [34]. Replacing the simple thresholding by more advanced segmentation approaches could prevent these misclassifications. Recent advances, such as machine learning—based segmentation methods, have been shown to provide accurate, observer-independent renal cortex segmentation [35].

Finally, the quantification of renal perfusion was performed using a simplified one-compartment model with a single post-labeling delay. Using a multi-parameter fitting model would capture more physiological detail, such as tissue heterogeneity and arterial transit times. However, this model is more sensitive to noise because it includes more variables. For this reason, and in line with the consensus recommendations, the simplified one-compartment model was chosen as a suitable method.

5.2 Renal Perfusion Results at 0.6 T

To acquire MR images at 0.6 T, the 3 T acquisition protocol was modified to account for the faster longitudinal relaxation and reduced SNR. Several parameters were adjusted and analyzed to determine the optimal acquisition settings that would result in the best perfusion images in terms of image quality and physiological accuracy. The strategy was to increase the voxel size and signal averaging to enhance the SNR, and adjust timing parameters (TR, PLD, and BGS) to compensate for the shorter T_1 . The influence of these modifications was assessed visually and qualitatively using tSNR. The tSNR was calculated from manually drawn regions of interest (ROIs) on the perfusion-weighted images.

This approach is straightforward but introduces potential bias because the manually defined ROIs are influenced by the visible perfusion contrast. Alternative methods, such as calculating tSNR based on an M_0 image or a T_1 map, could provide a more objective measurement. However, this requires precise image registration, which was not fully achieved in this project. Therefore, drawing a manual ROI on the PWIs was considered acceptable for this thesis.

A longer TR of 4000 ms allowed for more recovery time and produced visibly sharper kidney and cortico-medullary boundaries. A shorter TR led to blurring of structures and thus poorer delineation, likely because of incomplete longitudinal recovery. This insufficient recovery reduces the available magnetization, which decreases the perfusion-weighted difference signal. Quantitatively, the cortical tSNR nearly doubled when TR was lengthened from 3500 to 4000 ms for the same number of averages. For these reasons, a TR of 4000 ms was selected. Moreover, increasing the number of control-label pairs improved the tSNR of the cortex slightly, but this effect plateaued beyond 25 pairs. Therefore, 25 control-label pairs were selected.

One of the most impactful adjustments was the in-plane resolution. Increasing the voxel size from $3 \times 3 \text{ mm}^2$ to $4 \times 4 \text{ mm}^2$ markedly improved image SNR and quality. The 4 x 4 mm² resolution produced much clearer perfusion-weighted images, with welldefined boundaries for the kidney and between the cortex and medulla. The 3 x 3 mm² in-plane resolution resulted in a much noisier image, and the anatomical structures were harder to distinguish. The cortical tSNR of the left kidney increased from 0.44 at 3 mm in-plane to 0.72 at 4 mm. This observation is consistent with theoretical expectations, as increasing voxel size leads to a greater number of spins contributing to the signal. The trade-off, however, is a reduction in spatial resolution, which can introduce partial volume effects. As the consensus paper suggests a maximum in-plane of 4 mm, and that the image quality was superior at this resolution, $4 \times 4 \text{ mm}^2$ was chosen as the optimal size. Similarly, increasing the slice thickness from 8 mm to 10 mm provided a higher signal and a tSNR gain of 0.71 to 0.75. Both 8 mm and 10 mm slices produced usable perfusion maps, but 10 mm showed stronger signal. However, the 10 mm slice contains motion, which can complicate the comparison of these two thicknesses before registration. Given the improved SNR and the absence of noticeable partial volume effects, 10 mm slice thickness was chosen.

The PLDs of 1200, 1400, and 1800 ms were tested, each with the calculated optimal background suppression timings. At the shortest PLD, the PWI showed very high signal in the renal hilium and pelvis, which may indicate the labelled blood has not yet completely entered the renal parenchyma. Moreover, the kidney outlines and corticomedullary boundaries are poorly defined, especially in the right kidney. By increasing the PLD to 1400 ms, this macrovascular signal was reduced, but still present. With this PLD, the cortex and medulla are more distinguishable, and the overall renal outline is clearer (Figure 4.9b). This delay time was also used for 3 T, which is interesting, as a lower field strength would suggest a lower PLD due to the faster T_1 decay. The ASL consensus paper, published after the initiation of the NEO-2 study, recommends PLDs of 1600 –1800 ms. It is therefore possible that longer delays might have improved the quality of PWIs in the NEO-2 study. The PLD of 1800 shows a substantial signal loss and less well-defined kidney boundaries.

This indicates that the signal from the labeled blood decayed too much. Therefore, a PLD of 1400 ms was chosen.

A more precise approach to determine the optimal PLD would be to estimate the arterial transit time (ATT). As ATT varies between individuals (and even between cortex and medulla), measuring it directly would be more reliable. This can be achieved by acquiring data at multiple PLDs to derive a perfusion signal curve over time. This approach can provide more accurate values for PLD and improve the perfusion-weighted images. Therefore, a multi-PLD acquisition should be performed in future research.

After choosing a PLD of 1400 ms, two BGS schemes were evaluated. The first scheme used pulses at 700 and 1100 ms, which theoretically leaves 10-15% residual magnetization of static tissue. The second scheme used pulses at 670 & 1150 ms, which in theory should provide the most optimal suppression. Comparison of the PWI images acquired with different BGS pulse timings shows that the 700/1100 ms scheme resulted in improved suppression of static tissue. With this timing scheme, the background signal was reduced, the renal parenchyma appeared more clearly, and the whole-image tSNR was higher. The difference between the two schemes was most pronounced in the right kidney. The most likely reason is that the more aggressive 670/1150 timing, while theoretically driving the static magnetization as close to zero as possible in an ideal situation, may have driven some tissue components into slight negative magnetization. This leads to subtraction errors and thus suboptimal background suppression. Therefore, the 700 and 1100 ms BGS timing (with QUIPSS II saturation pulses at 200 and 100 ms before readout) was used in the final protocol.

Due to the limited time within this project, the readout strategy was not modified. However, besides an EPI readout, bSSFP is also an adequate alternative for 2D single-slice acquisitions in renal ASL-MRI [20]. The steady-state nature of bSSFP ensures that the available magnetization is used efficiently, resulting in relatively high SNR images. A limitation of this method is its sensitivity to field inhomogeneities. These effects are reduced at lower field strengths, making bSSFP an interesting parameter to research in future studies.

After evaluating all these parameters, the final 0.6 T ASL protocol used for part three consisted of: TR = 4000 ms, 25 label-control pairs, $4 \times 4 \text{ mm}^2$ in-plane resolution, 10 mm slice thickness, PLD = 1400 ms, and BGS pulses at 700 & 1100 ms.

5.3 Comparison of Renal Perfusion Results at 3 T and 0.6 T

Using the settings mentioned above, back-to-back scans were acquired in a healthy volunteer at the two field strengths to compare the perfusion results. The whole-kidney and cortical perfusion maps (with partial cortical segmentation) gave promising outcomes. The 0.6 T acquisition produced a clear perfusion map in which the cortex was clearly distinguishable as the region of highest signal.

As expected, the higher magnetic field strength resulted in an improved SNR at 3 T. The higher tSNR values indicate that the perfusion-weighted images acquired at this field strength are more reliable over time. This increased signal stability, combined with the sharper anatomical detail, results in noticeably higher image quality at 3 T. Nevertheless, the medullary signal distribution in the left kidney at 0.6 T showed a close resemblance to the 3 T reference. This suggests that, even with the lower SNR, ASL at 0.6 T may still be able to identify perfusion distributions.

Additionally, higher tissue contrast is observed in the 3 T images. This can be explained by the fact that T_2^* relaxation times decrease with increasing magnetic field strength, as magnetic field inhomogeneities scale with B_0 . These stronger local field gradients lead to faster intravoxel spin dephasing, resulting in a shorter T_2^* , and therefore increased T_2^* weighted contrast. On the other hand, clear EPI-related susceptibility distortions can be observed at 3 T in the phase-encoding direction, which are not visible at 0.6 T. These distortions are similar for M_0 and ASL images, so the quantified whole kidney perfusion values are reliable at 3 T. However, for automatic cortical perfusion quantification, the mid-field scanner would be particularly beneficial: the reduced geometric distortions could result in more accurate registration and thus more reliable cortical perfusion values.

Since a high-quality T_1 -weighted reference scan was not successfully acquired at 0.6 T (Figure 4.12), the cortical regions of interest had to be manually delineated on the perfusion maps themselves. This introduces potential observer and partial volume bias, as ROI placement may be influenced by visible perfusion contrast. Nevertheless, this approach still allowed for an approximate comparison with the 3 T data. For future research, acquiring a correct T_1 map at 0.6 T would allow for more consistent cortical segmentation and a more reliable comparison between scanners.

Despite these differences, the quantitative perfusion values measured at 0.6 T were remarkably close to the 3 T values for this subject. Cortical perfusion in the left kidney was 241.89 ± 76.55 mL/100g/min at 3 T and 215.34 ± 67.92 mL/100g/min at 0.6 T. For the right cortex, these values were 250.75 ± 70.82 at 3 T and 236.80 ± 66.33 mL/100g/min at 0.6 T. These small differences (approximately 5-10%) fall within the range of normal physiological and scanner-related variability [36, 37]. The difference in voxel size between the 0.6 T and 3 T protocols may also have contributed to this variation, as larger voxels increase partial volume effects and can lead to a slight underestimation of cortical perfusion.

These findings are based on a single-subject comparison and should therefore be seen as preliminary. Nevertheless, the results indicate that renal ASL at 0.6 T can quantify perfusion with values comparable to those obtained at 3 T. Future studies should include a larger number of subjects to confirm these observations.

Chapter 6

Conclusion

The three parts of this thesis have contributed to the standardization and progress of ASL-MRI for renal perfusion quantification.

1. Implementation and validation of a renal ASL analysis pipeline at 3 T.

The cortical perfusion values obtained from the post-processing pipeline were consistent with the physiological range reported in the literature. This step provided a reliable foundation for renal ASL analysis at 0.6 T. Future work could focus on further optimization of the registration steps and on the integration of automatic segmentation methods.

2. Acquisition and optimization of ASL data at 0.6 T.

For this project, the optimized ASL protocol at 0.6 T that provided the best image quality and quantitative performance included the following parameters: TR = 4000 ms, 25 label-control pairs, 4×4 mm² in-plane resolution, 10 mm slice thickness, PLD = 1400 ms, and background suppression pulses at 700 and 1100 ms. Future research could investigate alternative readout strategies such as bSSFP, which could provide relatively high SNR images.

3. Comparison of renal perfusion results between 3 T and 0.6 T.

The results demonstrate that renal ASL at 0.6 T can successfully quantify cortical perfusion with values comparable to those obtained at 3 T, with a difference of approximately 5-10%. In addition, reduced susceptibility artefacts at 0.6 T could provide more accurate perfusion quantification. To confirm these findings, a larger number of subjects should be scanned back-to-back at both field strengths.

Bibliography

- [1] C. P. Kovesdy, "Epidemiology of chronic kidney disease: An update 2022," *Kidney International Supplements*, vol. 12, no. 1, pp. 7–11, 2022. [Online]. Available: https://www.sciencedirect.com/science/article/pii/S2157171621000666
- [2] GBD Chronic Kidney Disease Collaboration, "Global, regional, and national burden of chronic kidney disease, 1990–2017: A systematic analysis for the global burden of disease study 2017," *The Lancet*, vol. 395, no. 10225, pp. 709–733, 2020.
- [3] A. Francis, M. N. Harhay, A. C. M. Ong, and et al., "Chronic kidney disease and the global public health agenda: an international consensus," *Nature Reviews Nephrology*, vol. 20, pp. 473–485, 2024. [Online]. Available: https://doi.org/10.1038/s41581-024-00820-6
- [4] J. M. ter Maaten, K. Damman, M. C. Verhaar, W. J. Paulus, D. J. Duncker, C. Cheng, L. van Heerebeek, H. L. Hillege, C. S. P. Lam, G. Navis, and A. A. Voors, "Connecting heart failure with preserved ejection fraction and renal dysfunction: the role of endothelial dysfunction and inflammation," *European Journal of Heart Failure*, vol. 18, no. 6, pp. 588–598, 2016.
- [5] A. R. Chade, "Small vessels, big role: Renal microcirculation and progression of renal injury," *Hypertension*, vol. 69, no. 4, pp. 551–563, Apr. 2017, epub 2017 Feb 13.
- [6] A. Bohle, S. Mackensen-Haen, and M. Wehrmann, "Significance of postglomerular capillaries in the pathogenesis of chronic renal failure," *Kidney & Blood Pressure Research*, vol. 19, pp. 191–195, 1996.
- [7] D. P. Kaufman, H. Basit, and S. J. Knohl, "Physiology, glomerular filtration rate," in *StatPearls*. Treasure Island (FL): StatPearls Publishing, 2023, pMID: 29763208. [Online]. Available: https://www.ncbi.nlm.nih.gov/books/NBK500032/

BIBLIOGRAPHY 39

[8] Y.-Z. Cai, Z.-C. Li, P.-L. Zuo, J. Pfeuffer, Y.-M. Li, F. Liu, and R.-B. Liu, "Diagnostic value of renal perfusion in patients with chronic kidney disease using 3d arterial spin labeling," *Journal of Magnetic Resonance Imaging*, vol. 46, no. 2, pp. 589–594, 2017.

- [9] F. Nery, E. De Vita, C. A. Clark, I. Gordon, and D. L. Thomas, "Robust kidney perfusion mapping in pediatric chronic kidney disease using single-shot 3d-grase asl with optimized retrospective motion correction," *Magnetic Resonance in Medicine*, vol. 81, no. 5, pp. 2972–2984, 2019.
- [10] C. Rossi, F. Artunc, P. Martirosian, H.-P. Schlemmer, F. Schick, and A. Boss, "Histogram analysis of renal arterial spin labeling perfusion data reveals differences between volunteers and patients with mild chronic kidney disease," *Investigative Radiology*, vol. 47, no. 8, pp. 490–496, 2012.
- [11] J. M. Mora-Gutiérrez, N. Garcia-Fernandez, M. F. S. Roblero, J. A. Páramo, F. J. Escalada, D. J. Wang, A. Benito, and M. A. Fernández-Seara, "Arterial spin labeling mri is able to detect early hemodynamic changes in diabetic nephropathy," *Journal of Magnetic Resonance Imaging*, vol. 46, no. 1, pp. 181–188, 2017.
- [12] G. Villa, S. Ringgaard, I. Hermann, R. Noble, P. Brambilla, D. S. Khatir, F. G. Zöllner, S. T. Francis, N. M. Selby, A. Remuzzi, and A. Caroli, "Phase-contrast magnetic resonance imaging to assess renal perfusion: a systematic review and statement paper," Magnetic Resonance Materials in Physics, Biology and Medicine, vol. 33, no. 6, pp. 885–899, 2019. [Online]. Available: https://link.springer.com/article/10.1007/s10334-019-00772-0
- [13] Q. Zhang, D. Wang, Y. Guo, L. Duan, and X. Zhang, "Application of noninvasive functional imaging to monitor the progressive changes in kidney diffusion and perfusion in contrast-induced acute kidney injury rats at 3.0 t," *Abdominal Radiology*, vol. 43, no. 4, pp. 775–781, 2018. [Online]. Available: https://link.springer.com/article/10.1007/s00261-017-1247-8
- [14] F. Zimmer, E. C. Nijssen, M. E. Gerlofs-Nijland, A. de Boer, A. van der Toorn, M. de Jong, R. J. Ploeg, H. van Goor, J. Grond, P. R. Luijten, B. J. van den Berg, and J. J. Zwanenburg, "Quantification of renal blood flow in rats using arterial spin labeling mri: influence of anesthesia and comparison with h₂¹⁵o-pet," Magnetic Resonance in Medicine, vol. 69, no. 2, pp. 560–566, 2013.
- [15] B. A. Alhummiany, D. Shelley, M. Saysell, M.-A. Olaru, B. Kühn, D. L. Buckley, J. Bailey, K. Wroe, C. Coupland, M. W. Mansfield, S. P. Sourbron, and K. Sharma, "Bias and precision in magnetic resonance imaging-based estimates of renal blood flow: Assessment by triangulation," *Journal of Magnetic Resonance Imaging*, vol. 55, no. 4, pp. 1241–1250, 2022.
- [16] R. S. Brown, M. Narayanan, J. L. Zhang et al., "The utility of magnetic resonance imaging for noninvasive evaluation of diabetic nephropathy," Nephrology Dialysis Transplantation, vol. 34, no. 6, pp. 929–936, 2019.

BIBLIOGRAPHY 40

[17] W. Mao, J. Zhou, M. Zeng, Y. Ding, L. Qu, C. Chen, X. Ding, Y. Wang, C. Fu, and F. Gu, "Intravoxel incoherent motion diffusion-weighted imaging for the assessment of renal fibrosis of chronic kidney disease: A preliminary study," *Magnetic Resonance Imaging*, vol. 45, pp. 153–159, 2018. [Online]. Available: https://doi.org/10.1016/j.mri.2017.12.010

- [18] D. R. Broome, "Nephrogenic systemic fibrosis associated with gadolinium-based contrast agents: A summary of 370 biopsy-confirmed cases," *Investigative Radiology*, vol. 43, no. 12, pp. 830–835, 2008.
- [19] M. R. Prince, H. L. Zhang, W. Chua-anusorn et al., "Risk factors for nsf: A literature review," *Journal of Magnetic Resonance Imaging*, vol. 30, no. 6, pp. 1298–1308, 2009.
- [20] F. Nery, C. E. Buchanan, A. A. Harteveld *et al.*, "Consensus-based technical recommendations for clinical translation of renal ASL MRI," *Magnetic Resonance Materials in Physics, Biology and Medicine*, vol. 33, pp. 141–161, 2020. [Online]. Available: https://doi.org/10.1007/s10334-019-00800-z
- [21] T. Rusche, J. Vosshenrich, D. J. Winkel, R. Donners, M. Segeroth, M. Bach, E. M. Merkle, and H.-C. Breit, "More space, less noise—new-generation low-field magnetic resonance imaging systems can improve patient comfort: A prospective 0.55t-1.5t-scanner comparison," *Journal of Clinical Medicine*, vol. 11, no. 22, p. 6705, Nov 2022.
- [22] T. Arnold, C. Freeman, B. Litt, and J. Stein, "Low-field mri: Clinical promise and challenges," *Journal of Magnetic Resonance Imaging*, vol. 57, no. 1, pp. 25–44, 2023.
- [23] T. Rusche, H.-C. Breit, M. Bach, J. Wasserthal, J. Gehweiler, S. Manneck, J.-M. Lieb, G. M. De Marchis, M. N. Psychogios, and P. B. Sporns, "Potential of stroke imaging using a new prototype of low-field mri: A prospective direct 0.55 t/1.5 t scanner comparison," *Journal of Clinical Medicine*, vol. 11, no. 10, p. 2798, May 2022.
- [24] M. K. Stehling, R. Turner, and P. Mansfield, "Echo-planar imaging: magnetic resonance imaging in a fraction of a second," *Science*, vol. 254, no. 5028, pp. 43–50, Oct 1991.
- [25] W.-C. Wu, M.-Y. Su, C.-C. Chang, W.-Y. I. Tseng, and K.-L. Liu, "Renal perfusion 3-t mr imaging: A comparative study of arterial spin labeling and dynamic contrastenhanced techniques," *Radiology*, vol. 261, no. 3, pp. 845–853, 2011.
- [26] A. A. Harteveld, A. de Boer, S. L. Franklin, T. Leiner, M. van Stralen, and C. Bos, "Comparison of multi-delay fair and peal labeling approaches for renal perfusion quantification at 3t mri," *Magnetic Resonance Materials in Physics, Biology and Medicine*, vol. 33, pp. 81–94, 2020.
- [27] C. E. Buchanan, E. F. Cox, and S. T. Francis, "Evaluation of 2d imaging schemes for pulsed arterial spin labeling of the human kidney cortex," *Diagnostics*, vol. 8, no. 3, p. 43, 2018.

BIBLIOGRAPHY 41

[28] C. A. Olman, L. Davachi, and S. Inati, "Distortion and signal loss in medial temporal lobe," *PLoS ONE*, vol. 4, no. 12, p. e8160, 2009. [Online]. Available: https://doi.org/10.1371/journal.pone.0008160

- [29] I. Brumer, D. F. Bauer, L. R. Schad, and F. G. Zöllner, "Synthetic arterial spin labeling mri of the kidneys for evaluation of data processing pipeline," *Diagnostics*, vol. 12, no. 8, p. 1854, 2022. [Online]. Available: https://doi.org/10.3390/diagnostics12081854
- [30] R. Henry and et al., "Mri quantitative t1 and t2 mapping of the renal cortex: Assessment of normal values and potential usefulness for renal masses at 3 t," European Journal of Radiology, vol. 181, p. 111741, 2024. [Online]. Available: https://www.sciencedirect.com/science/article/pii/S0720048X24004571
- [31] H. K. Moorthy and P. Venugopal, "Measurement of renal dimensions in vivo: A critical appraisal," *Indian Journal of Urology*, vol. 27, no. 2, pp. 169–175, 2011. [Online]. Available: https://www.ncbi.nlm.nih.gov/pmc/articles/PMC3142824/
- [32] A. E. Campbell-Washburn, R. Ramasawmy, M. C. Restivo, I. Bhattacharya, B. Basar, D. A. Herzka, M. S. Hansen, T. Rogers, W. P. Bandettini, D. R. McGuirt et al., "Opportunities in interventional and diagnostic imaging by using high-performance low-field-strength mri," Radiology, vol. 293, pp. 384–393, 2019. [Online]. Available: https://pubs.rsna.org/doi/full/10.1148/radiol.2019190628
- [33] A. Odudu, F. Nery, A. A. Harteveld, R. G. Evans, D. Pendse, C. E. Buchanan, S. T. Francis, and M. A. Fernández-Seara, "Arterial spin labelling mri to measure renal perfusion: a systematic review and statement paper," Nephrology Dialysis Transplantation, vol. 33, pp. ii27–ii35, 2018. [Online]. Available: https://doi.org/10.1093/ndt/gfy180
- [34] J. Wu, Z. Shi, Y. Zhang, J. Yan, F. Shang, Y. Wang, H. Lu, H. Gu, W. Dou, X. Wang, and L. Yuan, "Native T1 mapping in assessing kidney fibrosis for patients with chronic glomerulonephritis," *Frontiers in Medicine*, vol. 8, p. 772326, Oct. 2021. [Online]. Available: https://doi.org/10.3389/fmed.2021.772326
- [35] I. K. Bones, C. Bos, C. Moonen, J. Hendrikse, and M. van Stralen, "Workflow for automatic renal perfusion quantification using asl-mri and machine learning," *Magnetic Resonance in Medicine*, vol. 87, no. 2, pp. 800–809, Feb. 2022. [Online]. Available: https://doi.org/10.1002/mrm.29016
- [36] A. de Boer, A. A. Harteveld, B. Stemkens, P. J. Blankestijn, C. Bos, S. L. Franklin, M. Froeling, J. A. Joles, M. C. Verhaar, N. van den Berg, H. Hoogduin, and T. Leiner, "Multiparametric renal mri: An intrasubject test-retest repeatability study," *Journal of Magnetic Resonance Imaging*, vol. 53, no. 3, pp. 859–873, Mar. 2021, epub 2020 Apr 16.
- [37] M. Cutajar, D. L. Thomas, T. Banks, C. A. Clark, X. Golay, and I. Gordon, "Repeatability of renal arterial spin labelling mri in healthy subjects," *MAGMA*, vol. 25, no. 2, pp. 145–153, Apr. 2012.

APPENDICES

Appendix A

Parameter Text File

The affine registration parameter text file from the University of Heidelberg used in the registration step is provided below. The parameters that were changed for this thesis are shown in bold.

```
(FixedImageDimension 2)
(MovingImageDimension 2)
(UseDirectionCosines "true")
(Registration "MultiResolutionRegistration")
(Interpolator "BSplineInterpolator")
(ResampleInterpolator "FinalBSplineInterpolator")
(Resampler "DefaultResampler")
(Optimizer "StandardGradientDescent")
(Transform "AffineTransform")
(Metric "AdvancedMattesMutualInformation")
(AutomaticScalesEstimation "true")
(AutomaticTransformInitialization "true")
(HowToCombineTransforms "Compose")
(FinalGridSpacingInVoxels 16)
(NumberOfMovingHistogramBins 32)
(NumberOfFixedHistogramBins 32)
(ErodeMask "true")
(NumberOfResolutions 4)
(ImagePyramidSchedule 8 8 4 4 2 2 1 1)
(MaximumNumberOfIterations 400)
(NumberOfSpatialSamples 1000)
(NewSamplesEveryIteration "true")
```

```
(ImageSampler "RandomCoordinate")
(BSplineInterpolationOrder 1)
(FinalBSplineInterpolationOrder 3)
(DefaultPixelValue 0)
(WriteResultImage "true")
(ResultImagePixelType "float")
(ResultImageFormat "nii")
(SPalpha 0.600000)
(SPA 50)
(WriteTransformParametersEachIteration "false")
(WriteTransformParametersEachResolution "false")
(ShowExactMetricValue "false")
(FixedInternalImagePixelType "float")
(MovingInternalImagePixelType "float")
(CompressResultImage "false")
```

Note: (ResultImagePixelType "float") and (ResultImageFormat "nii") were chosen to store the results as NIfTI files with floating-point precision. The single-file .nii format also simplifies data handling compared to the two-file .mhd/.raw structure.

Appendix **B**

Literature Review

Quantifying Renal Perfusion with Arterial Spin Labeling (ASL) - A Comparison Across ASL Techniques and DCE-MRI

W. Deen¹, B. Siadari², M. Nagtegaal², T. van Osch², H. Lamb², R. Remis¹, I. Dekkers²

¹ Technical University of Delft, ² Leiden University Medical Centre (LUMC)

Abstract

Chronic kidney disease (CKD) affects more than one in ten individuals worldwide and has a high mortality rate. The estimated glomerular filtration rate (eGFR) is widely used for diagnosis, but this diagnostic tool lacks sensitivity in early-stage CKD. Arterial spin labeling (ASL) MRI is a promising alternative as it can non-invasively image renal perfusion. This literature review examines studies comparing ASL MRI and other MRI-based perfusion techniques. Seven studies met the inclusion criteria: three comparing ASL and dynamic contrast-enhanced (DCE) MRI, and four evaluating different ASL methodologies. Higher perfusion values are reported with DCE-MRI, though often without statistical significance. In a ddition, ASL MRI demonstrates better reproducibility. However, the variability in methodology across studies and differences in anatomical and physiological factors between and within subjects make the comparison less reliable. This review shows the potential of ASL MRI for quantifying renal perfusion, but methodological standardization is needed to support its clinical validation.

Key words. Arterial Spin Labeling, Kidney Imaging, Magnetic Resonance Imaging, Renal Perfusion.

1. INTRODUCTION

Chronic kidney disease (CKD) affects more than one in ten individuals worldwide and has a high mortality rate. CKD can lead to end-stage renal disease (ESRD). At this advanced stage, the kidney function has deteriorated to such an extent that dialysis or transplantation is required. Estimates suggest that by 2040, CKD may be responsible for 2.2 to 4.0 million deaths [9]. In addition, impaired renal function increases the risk of cardiovascular disease. Deaths from CKD and cardiovascular complications linked to renal dysfunction represented 4.6% of global mortality [13].

Currently, estimated glomerular filtration rate (eGFR) is used to diagnose CKD [12]. However, eGFR lacks sensitivity for detecting early-stage CKD, as advanced pathological damage may already be present when only slight decreases of eGFR are observed [8, 11, 15, 22]. As a result, using eGFR as a diagnostic marker for CKD often leads to underdiagnosis of this disease. Accelerating the diagnosis is crucial, as it enables early intervention and can therefore reduce or prevent disease progression. A possible early detection indicator of renal function is

kidney perfusion, defined as blood flow per 100 grams of renal tissue per minute (mL/100g/min). Reduced cortical perfusion in patients with CKD has been reported across several studies [5, 19, 25], with the degree of reduction varying by disease stage [18]. The quantification of cortical perfusion could thus be a valuable method for diagnosing early-stage CKD.

Various imaging techniques have been used to assess renal perfusion, including positron emission tomography (PET), computed tomography (CT), and magnetic resonance imaging (MRI). As these techniques have limitations, there is still no gold standard technique available for quantifying renal perfusion. PET and CT expose patients to ionizing radiation, whereas MRI is a radiation-free alternative. Several MRI techniques have been used to measure renal perfusion, including dynamic contrast-enhanced (DCE) imaging, arterial spin labeling (ASL), and intravoxel incoherent motion diffusion-weighted imaging (IVIM-DWI) [27, 30, 31]. The quantification of renal perfusion with these MRI methods has demonstrated promising results in detecting kidney dysfunction and disease [1, 3, 16, 27].

ASL MRI is an MRI technique that magnetically labels arterial blood water using radiofrequency (RF) inversion pulses. Unlike other MRI techniques, this technique is non-invasive as it uses an endogenous tracer, which means no contrast agent is required. This characteristic is particularly advantageous for patients with compromised kidney function, who may be at increased risk for complications associated with contrast agent administration, such as nephrogenic systemic fibrosis (NSF) [2, 23]. In addition to being non-invasive, ASL MRI can provide structural and regional information on renal perfusion. This review aims to examine all available studies comparing different ASL MRI techniques with each other and with other MRI-based perfusion methods for measuring renal perfusion.

2. METHODS

2.1. Data collection

This systematic review was conducted according to Preferred Reporting Items for Systematic Reviews and Meta-Analyses (PRISMA) guidelines [26]. A literature search was conducted in PubMed on 1 February 2025 using a combination of Medical Subject Headings (MESH terms) and free text including terms. To identify additional relevant publications not retrieved from PubMed, adjusted queries were also applied to Web of Science and Embase (Ovid) databases. The search strategy included terms related to renal blood flow, renal perfusion, ASL MRI, DCE-MRI, DWI, and IVIM. The final queries can be found in Appendix A and were validated by the medical librarian at LUMC and a PhD candidate specializing in renal perfusion imaging.

2.2. Screening process

The screening process was conducted using Rayyan, an AI-powered platform for systematic reviews [21], by reviewing the titles and abstracts of the articles. Only English-language publications reporting quantitative renal ASL perfusion values compared to other MRI techniques were included. Studies that compared ASL perfusion values with non-MRI techniques or those lacking a comparative modality were excluded from the main analysis. However, they were used to support the background context of this systematic review. Once the initial screening process was completed, a random quality check on 10% of the screened articles was performed by the previously mentioned PhD candidate. Final inclusion decisions were made in consensus between the PhD candidate and the lead reviewer. During this phase, animal articles were excluded, as their renal perfusion values were not comparable to the human values.

2.3. Data extraction and outcomes

For each included study, the following characteristics were extracted: participant demographics (age,

sample size, health status), MRI technical parameters (field strength, labeling method, acquisition and readout scheme), whether a distinction between cortex and medulla was made, and renal perfusion values. These key findings were presented in an overview table accompanied by a description of the results. As secondary outcomes, studies that reported signal-to-noise ratio (SNR) and repeatability or reproducibility metrics were also analyzed and discussed.

2.4. Quality assessment

The eligible articles were assessed using a modified version of the National Institute of Health quality assessment tool for observational cohort and cross-sectional studies (NHLBI). This adapted tool consisted of eight questions and is provided in Appendix B. Each "Yes" response was assigned 1 point, and "No", "Cannot Determine", and "Not Reported" received 0 points. Studies scoring under 50% were classified as having "poor" quality and excluded.

3. RESULTS

The database search resulted in a total of 1,272 articles. The flowchart of the screening process can be found in Figure 1. In total, seven articles met the inclusion criteria. Of these, three compared ASL MRI to DCE-MRI, and four compared different ASL techniques. All included studies were rated above the 50% quality threshold. The answers to the quality assessment tool and corresponding scores are presented in Appendix C.

3.1. Study characteristics

The most important study characteristics are presented in Tables 1 and 2. Table 1 provides a summary of the studies comparing DCE with ASL, and Table 2 summarizes the findings from the studies comparing within ASL techniques. This systematic review included 165 participants between 23 and 72 years of age. The studies were generally small, ranging from 8 to 66 participants, with two studies using a 1.5 T scanner and five 3 T scanners. Four studies compared ASL techniques, of which two compared pulsed arterial spin labeling with flow-sensitive alternating inversion recovery (PASL-FAIR) to pseudo-continuous arterial spin labeling (pCASL), one evaluated different readout techniques within PASL-FAIR, and one compared 2D to 3D pCASL. PASL-FAIR and pCASL differ in their labeling techniques: PASL-FAIR applies short, spatially selective inversion pulses, whereas pCASL uses a train of radiofrequency pulses to continuously label inflowing blood. The remaining three included studies compared ASL (two using pCASL and one PASL-FAIR) to DCE-MRI. Four studies included hydration or diet instructions before scanning [1, 4, 6, 10].

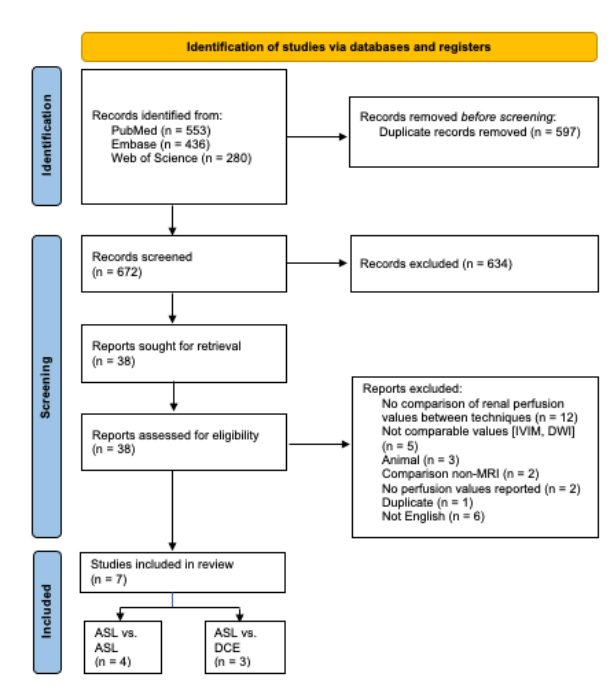


Fig. 1: PRISMA flow diagram of studies identified and included.

3.2. ASL MRI

Across the included studies, five used pCASL [1, 24, 29, 14, 10] and three used PASL-FAIR [6, 10, 14].

3.2.1. pCASL

Of the five articles discussing pCASL, four used pCASL with a labeling duration of 1.5 seconds and a postdelay of 1.5 seconds [1, 10, 14, 24]. In addition to the postdelay of 1.5 seconds, the study by Harteveld et al. also used delays of 0.5, 1.0, and 2.0 seconds [10]. The only study that differed in terms of postdelay used a delay of 1.0 second and a labeling duration of 1.5 seconds, with labeling applied 70-90 mm above the center of the imaging volume [29]. Among the studies that reported labeling position, this ranged between 70 and 110 mm above the kidneys [1, 10, 29].

Four studies reported using single-shot acquisitions [10, 14, 24, 29], one of which also included multi-shot acquisitions. Two of the studies solely acquiring single-shot images both used gradient-echo (GRE) echo-planar-imaging (EPI) for readout [10, 29], whereas the study by Robson et al. utilized a 3D fast spin echo (FSE) sequence. In the study by Lu et al, single-shot acquisition was performed with Turbo Gradient Spin Echo (TGSE) readout [14], which was also used in the study by Alhummiany et al.

Two studies used Buxton's kinetic model to calculate renal perfusion [1, 10]. The remaining three studies also relied on parameters used in Buxton's formu-

las, such as the difference in magnetization between the labeled and non-labeled images, the tissue-blood partition coefficient (λ) , inversion efficiency (α) , and T_1 relaxation times. However, Wu et al. did not account for the arterial transit time (ATT), a parameter included in Buxton's original model. The studies by Lu et al. and Robson et al. both incorporate specific parameters tailored to the labeling techniques for renal perfusion.

3.2.2. PASL-FAIR

Four studies used a PASL-FAIR labeling scheme, of which two compared pCASL to PASL-FAIR, one compared PASL-FAIR to DCE, and one compared different readout techniques within PASL-FAIR [4, 6, 10, 14].

The studies by Harteveld et al. and Lu et al. used the same readout scheme as with pCASL: single-shot 2D GRE EPI and single-shot 3D TGSE, respectively. The study by Cutajar et al., which compares the PASL-FAIR technique to DCE-MRI, used a multi-shot 3D GRASE imaging module. Buchanan et al. compared four readout techniques: Balanced Fast Field Echo (bFFE), GRE EPI, SE-EPI, and Turbo Spin Echo (TSE), also known as single-shot TSE.

The time-to-inversion (TI) values used in these studies ranged between 0.8 and 2.7 seconds. Two studies used multiple TI values [6, 10], while two others used a single TI value [4, 14].

In two studies, the bolus duration (τ) was assumed $(\tau = 0.7 \text{ s} \text{ and } \tau = 1.2 \pm 0.2 \text{ s})$, whereas the study by Harteveld et al. controls this parameter with the QUIPSS II scheme, resulting in $\tau = 1.2 \text{ s}$ [6, 10, 14].

Three studies specifically used Buxton's kinetic model for the calculation of renal perfusion [4, 6, 10]. Of these three, the study by Cutajar et al. mentions a more simplified version of Buxton's model as it assumes instantaneous exchange of labeled blood water upon arrival of the bolus. The fourth study did not explicitly mention Buxton's model but uses parameters from this model [14].

3.3. DCE-MRI

Of the three included studies using DCE-MRI, two used 3 T scanners and one a 1.5 T scanner. DCE-MRI uses a dose of contrast injected intravenously to enhance signal intensity in tissues of interest, which enables the acquisition of dynamic images. All the studies used a gradient-echo-based readout to acquire the datasets, of which two used a FLASH sequence [6, 29].

Two studies used a similar pipeline to calculate the renal perfusion [1, 6]. The first step was deriving the arterial input function (AIF), defined the contrast concentration in the aorta over time, and tissue intensity signal extraction (using ROI segmentation), which shows how the contrast agent moves through the kidney. Subsequently, these parameters are converted to concentration curves. Lastly, compartment modeling is done to get the perfusion values.

In the study by Alhummiany et al., a two-compartment filtration kinetic model was used, whereas Cutajar et al. used the Toft two-compartment model. These studies used the Platform for Medical Imaging (PMI) 0.4 software package to analyze the DCE datasets [1, 6]. The third study on DCE-MRI calculated the renal perfusion by deconvolving the tissue concentration-time curve (cortex or medulla) with the abdominal aorta, which is defined as AIF in this study [29].

3.4. Renal perfusion

Five studies reported the renal cortical perfusion [6, 10, 14, 24, 29], of which three additionally reported the medullar renal perfusion [10, 14, 29]. One study reported the renal perfusion values for the whole kidney [1].

The results of the three studies comparing DCE-MRI and ASL MRI are summarized in Table 1. Overall, DCE-MRI reported higher perfusion values across the cortex, medulla, and whole kidney. However, only one study demonstrated a statistically significant difference between the two techniques [29]. Two studies mentioned cortical perfusion values with ASL-and DCE-MRI: 236±46 vs. 227±30 ml/100 g/min and 287±79 vs. 272±50 ml/100 g/min, respectively [6, 29].

Table 2 presents the renal perfusion values reported in studies comparing ASL techniques. Renal cortical perfusion in healthy participants by all ASL techniques ranged from 200±20 mL/100g/min to 367.7±63.8 mL/100g/min, showing a wide variation of values. Renal medullar perfusion values in healthy participants ranged from 84±27 ml/100g/min to $222.1\pm46.3 \text{ ml}/100 \text{g/min}$. The difference between the values was negligible in the study by Robson et al., suggesting that acquisition dimensionality may not affect renal perfusion values. In contrast, the other three studies reported varying values between techniques [4, 10, 14]. Harteveld et al. reported lower cortical perfusion with pCASL, whereas Lu et al. found slightly higher cortical perfusion values with this technique in healthy volunteers. Buchanan et al. noted that cortical perfusion values were higher for gradient-echo schemes (GE-EPI and bFFE) compared to spin-echo-based schemes (SE-EPI and TSE) within the FAIR technique [4].

3.5. SNR

Five studies reported values related to the signal-tonoise ratio (SNR) [4, 10, 14, 24, 29]. Among these, three explicitly reported SNR [14, 24, 29], one focused on temporal SNR (tSNR) [10], and one study provided both SNR and tSNR values [4]. One study presented the tSNR values graphically, demonstrating an overall higher tSNR for PASL-FAIR [10] compared to pCASL. The study by Lu et al. reported significantly higher cortical SNR values for healthy participants using pCASL compared to PASL-FAIR [14]. Robson et al. reported average SNR values for the different acquisition methods, which varied in slice thickness. The SNR values reported were 4.7 ± 1.9 for 3D FSE with 2.8 mm thickness, 8.2 ± 3.3 and 6.0 ± 2.0 for 3D FSE with 11.2 mm thickness, and 9.2 ± 3.1 for 2D ss-FSE with 10 mm thickness. Although 3D FSE values were higher with synchronized breathing compared to free breathing, the differences were not statistically significant. Buchanan et al. [4] evaluated perfusionweighted image SNR (PWI-SNR) and tSNR across four acquisition techniques: bFFE, GE-EPI, SE-EPI, and TSE. The values ranged from 4.9 ± 1.5 (SE-EPI) to 8.5 ± 4.1 (TSE) for PWI-SNR and from 1.5 ± 0.8 (GE-EPI) to 2.6 ± 1.6 (SE-EPI) for tSNR. Notably, the SE-EPI has the lowest PWI-SNR and the highest tSNR. Although one study reported SNR values for the ASL technique, these were limited to comparisons between the cortex and medulla, rather than between DCE- and ASL MRI [29]. Additionally, this study presented temporal contrast-to-noise ratio (tCNR) values for DCE-MRI, but these parameters are not directly comparable.

3.6. Repeatibility

All studies reported metrics regarding repeatability, including the Intraclass Correlation Coefficient (ICC) and the Coefficient of Variation (CV). In the three studies that compare ASL MRI to DCE-MRI, two reported lower within-subject CVs for ASL, which indicates superior repeatability [6, 29]. Cutajar et al. reported CVs ranging from 14% to 18% (right and left kidney, respectively) for ASL and 27% to 32% (right and left kidney, respectively) for DCE. Similarly, Wu et al. reported cortical and medullary CVs of 7.9% and 7.2% for ASL, respectively, compared to 9.6% and 19.1% for DCE. Alhummiany et al. reported a relative repeatability error (RRE) of 61% for perfusion measurement with ASL. This study stated that this corresponds to a CV of approximately 31% when divided by 1.96, which is higher than the other two studies. Although this study also provided repeatability values for phase-contrast (PC) MRI, these values were not considered in the current review, as the primary outcome for this technique was not mentioned.

The outcomes of the studies that analyzed different ASL techniques lack a clear pattern. According to Harteveld et al., PASL-FAIR showed better repeatability than pCASL, with higher ICC values and lower CVs across all measurements. For example, the cortical CVs was 9.9% for FAIR versus 33.9% for pCASL. Lu et al. assessed repeatability using intra- and interobserver ICCs in CKD patients (both more than 0.9) but did not provide CVs for healthy volunteers. This study showed slightly higher ICC values for pCASL,

Table 1: Overview of studies comparing different ASL techniques for renal perfusion quantification (mL/100g/min).

Category		Harteveld	Lin	Bobson	Buchanan
Cace of the cace o			3	1100001	
Disease		1	CKD	RCC	
Participants (p/c)		16 (-/16)	66 (48/18)	8 (4/4)	10 (-/10)
Age(y)		51 ± 10	42.9 ± 10.8	23-53 (c), $39-67$ (p)	27 ± 10
Field strength (T)		3.0	3.0	1.5	3.0
Labeling L1		PASL-FAIR	PASL-FAIR	3D-pCASL	PASL-FAIR
Readout L1		$_{ m ss}$ GRE-EPI †	3D-TGSE	3D-FSE	$\mathrm{GRE} ext{-}\mathrm{EPI}^\dagger+\mathrm{bFFE}^\dagger$
Labeling L2		$_{ m pCASL}$	$_{ m pCASL}$	2D- $pCASL$	PASL-FAIR
Readout L2		$_{ m ss}~{ m GRE-EPI}^{\dagger}$	3D-TGSE	2D-FSE	$\mathrm{SE} ext{-}\mathrm{EPI}^{\ddagger}+\mathrm{TSE}^{\ddagger}$
Background suppression		$\mathrm{Yes}\;(\mathrm{QUIPSS\;II})$	Yes	Yes	Yes (WET $+$ sinc)
Labeling duration L1 (ms)		Inst. (PASL)	Inst. (PASL)	1500	Inst. (PASL)
Labeling duration L2 (ms)		1500	1500	1500	Inst. (PASL)
PLD L1 (ms)		800-2600	800-2600	1500	1300/1800
PLD L2 (ms)		500-2000	1500	1500	
Number of averages		10	20	16 (2D), 1 (3D)	25
Quantification model L1		General kinetic	FAIR specific	pCASL specific (same)	General kinetic
Quantification model L2		General kinetic	pCASL specific	pCASL specific (same)	General kinetic
Renal Perfusion L1 (mL/100g/min)	Patients	•	$307.1 \pm 76.4 (C)$		
			$184.3 \pm 59.1 \text{ (M)}$		
	Controls	$362 \pm 57 (C)$	$367.7 \pm 63.8 \text{ (C)}$	$284 \pm 21 \text{ (C)}$	$276 \pm 29 \; (\mathrm{bFFE}, \mathrm{C})$
		$140 \pm 47 \; (M)$	$222.1 \pm 46.3 \text{ (M)}$		$222 \pm 18 \text{ (GRE-EPI, C)}$
					$201 \pm 36 \text{ (SE-EPI, C)}$
					$200 \pm 20 \; (TSE, C)$
Renal Perfusion L2 $(mL/100g/min)$	Patients	ı	$259.5 \pm 82.1 (C)$	-	ı
			$147.0 \pm 52.2 \text{ (M)}$		
	Controls	$201 \pm 72 (C)$	$375 \pm 32.2 \text{ (C)}$	$282 \pm 21 \text{ (C)}$	
		$84\pm27~(\mathrm{M})$	$225.5 \pm 23.1 \text{ (M)}$		

 $p=patients,\ c=controls,\ C=cortex,\ M=medulla;\ CKD=chronic\ kidney\ disease;\ RCC=renal\ cell\ carcinoma;\ PLD=post-labeling\ delay;$ Inst. = Instantaneous.

 $QUIPSS\ II = bolus\ control\ technique\ for\ PASL;\ WET = water\ suppression\ technique;\ sinc = sinc\ post-saturation\ pulse.$ † Gradient-echo readouts: bFFE, GRE-EPI.

Spin-echo readouts: SE-EPI, TSE.

Table 2: Overview of studies comparing ASL techniques with DCE-MRI for renal perfusion quantification (mL/100g/min).

Category	Cutajar	Alhummiany					
Disease	-		T2DM				
Participants (p/c)	16 (-/16)	19 (-/19)	30(25/5)				
Age (y)	23-40	25–68	31-72				
Field strength (T)	1.5 3.0		3.0				
ASL Specifc Parameters							
Labeling	PASL-FAIR	pCASL	pCASL				
Background suppression	Yes (QUIPSS II)	No	Yes				
Labeling duration (ms)	Inst. (PASL)	1500	1500				
PLD (ms)	100-2700	1000	1500				
Number of averages	Not reported	10×6 (first 2 discarded)	Not reported				
Readout	ms-GRASE	ssGRE-EPI	3D-TGSE				
Quantification model	General kinetic	One-compartment	General kinetic				
DCE Specific Parameters							
Contrast agent	Gd-DOTA	Gadopentetate	Gd-DOTA				
Dose (mmol/kg)	0.05	0.0125	0.025				
Injection rate (mL/s)	2	4	2				
Saline flush (mL)	15	-	20				
Readout	3D-FLASH	tFLASH	2D-Turbo FLASH				
Quantification model	Tofts two-	Deconvolution	Two compartment				
dantinication model		(concentration—time curve)	filtration				
Renal Perfusion ASL (mL/100g/min)							
Patients	-	_	$146 \pm 22 \; (W)$				
Controls	$236 \pm 46 \text{ (C)}$	227 ± 30 (C), 101 ± 21 (M)	$155 \pm 50 \ (W)$				
Renal Perfusion DCE (mL/100g/min)							
Patients	- 1	-	$214 \pm 31 \; (W)$				
Controls	$287 \pm 79 \; (C)$	$272 \pm 60 \text{ (C)}, 122 \pm 30 \text{ (M)}$	- ` ′				

p = patients, c = controls, C = cortex, M = medulla, W = whole kidney; T2DM = type 2 diabetes mellitus; PLD = post-labeling delay; Inst. = Instantaneous. QUIPSS II = bolus control technique for PASL.

which contradicts the results from Harteveld et al.

Buchanan et al. evaluated the CVs for four acquisition techniques within PASL-FAIR and identified the SE-EPI readout scheme as most repeatable (CV = 17.2~%). They also showed there was no significant difference between the first and second visits of each readout scheme, which indicates good repeatability for PASL-FAIR. Lastly, Robson et al. investigated 3D FSE pCASL test-retest and reported a CV of 8.8%, the lowest among all reviewed studies.

4. DISCUSSION

The initial search query for this literature review aimed to collect articles comparing ASL MRI techniques with other MRI techniques. After examining the retrieved articles, studies using parameters not comparable to ASL-derived perfusion values were excluded. This resulted in an inclusion of articles com-

paring ASL techniques with each other and ASL with DCE-MRI techniques for quantifying renal perfusion. While both methods aimed to assess the hemodynamics of the kidney, the studies included in this review demonstrate that direct perfusion value comparison with ASL and DCE and within ASL is complicated due to methodological and physiological variability.

4.1. ASL MRI

The studies comparing the ASL techniques did not show a consistent pattern in the reported perfusion values. This variation is also seen in an animal study comparing the perfusion values across different coil sizes used: while FAIR showed higher perfusion values compared to pCASL for a 5x3 cm2 coil, FAIR performance decreased significantly with the smaller coil, whereas pCASL maintained its performance [7]. These inconsistencies show the influence of variations within the same MRI technique. Acquisition param-

eters such as field strength, labeling strategy (e.g., pCASL vs PASL-FAIR), post-labeling delay, background suppression, and readout type (2D vs 3D, EPI vs FSE) significantly influence the ASL signal and, consequently, perfusion estimates. This methodological sensitivity was evident in Harteveld's and Lu's studies, where different ASL approaches led to systematically higher or lower perfusion values [10, 14]. In several studies, technical parameters specific to the ASL sequence, such as labeling efficiency (α) and arterial transit time (ATT), were either assumed or not measured individually. This limitation contributes to variability in perfusion estimates. To improve reliability of the imaging method, Harteveld et al. used multi-delay ASL, which captures the dynamic inflow of labeled flow, and implemented QUIPSS II to control bolus duration. This combination improved precision of the method and, in turn, the accuracy of the perfusion outcomes. However, this was not uniformly done in the other studies.

In addition to acquisition parameters, quantification choices also affect results. The quantification model used in several studies in this review is (based on) the Buxton general kinetic model [1, 6, 10]. This model requires input parameters such as labeling efficiency α , tissue-blood partition coefficient λ , and bolus duration τ . In the majority of the studies, these parameters were assumed or estimated based on literature values, rather than being directly measured, which introduces unreliability. Labeling efficiency (α) , for example, may vary between individuals and across repeated measurements within the same subject due to physiological factors such as aortic flow velocity. Thus, if this parameter is assumed instead of measured, the outcomes are less reliable. Moreover, labeling efficiency (α) is sensitive to the homogeneity of the magnetic fields B_0 and B_1 , which also depends on scanner hardware. B_0 and B_1 inhomogeneities at the labeling location are known to reduce the labeling efficiency α [10, 29]. In the study by Harteveld et al., relatively low perfusion values were observed with pCASL, despite its higher temporal SNR compared to FAIR. This study suggested that this notable observation could be attributed to the inhomogeneities.

Beyond the methodology aspect, anatomical and physiological factors of the kidney also influence these differences. The kidney has a unique perfusion architecture: approximately 90% of renal blood flow is directed to the cortex, while only 10% perfuses the medulla [17]. ASL, which is particularly sensitive to low flow due to T_1 dependency and long transit times, can underrepresent the medullary perfusion. If one method targets a slightly different region within the kidney than another, differences in measurements will arise. For example, partial-volume effects in DCE imaging could lead to the inclusion of some medullary signal, whereas an ASL ROI might be restricted to the cortex. This would result in lower ASL values, not due to inaccuracy but due to ROI definition. Another

anatomical constraint is the overlapping of labeling and the abdominal aorta. Excluding this region from the inversion volume in individuals with kidneys situated at or near the level of the aorta is technically hard. As the quantification model assumes that the labeling volume (selective inversion slab) is spatially separate from the imaging volume, an overlap in these slabs can result in an overestimation of renal perfusion. Additionally, variable hydration status, blood pressure, arterial transit times, and kidney motion between and within subjects may affect the outcomes. Delayed arterial transit, which can be occur in the elderly or those with pathological kidneys, may lead to underestimation. In DCE, the contrast delivery to tissue is simply delayed under these conditions, and for ASL, underestimation occurs when the post-label delay is insufficient. Kidneys move with respiration, which further complicates the perfusion quantification. Techniques that effectively compensate for motion with methods such as background suppression, triggering, image registration, will produce more reliable images. The differences in motion correction methods can affect the perfusion outcomes.

Overall, the variations show that comparing perfusion values across the methods is unreliable. The lack of standardization has been a barrier, as addressed by PARENCHIMA [20], which tries to overcome this limitation by proposing a protocol for the technique.

4.2. DCE-MRI

A uniform finding across the included studies is that DCE-derived perfusion values are slightly higher than those measured by ASL. However, since this observation is based on only three comparative studies, the conclusion should be considered preliminary and compared with existing literature. A similar pattern was observed in an animal study that showed systematically (non-significantly) higher DCE values for the cortex [31]. In contrast, another animal study found close agreement between ASL and ROI based DCE, with slightly higher values using ASL [28]. However, this study also measured perfusion with DCE pixel-wise and shows higher values with this segmentation technique than with ASL. The difference between ROI-based DCE and pixel-wise DCE was significant, emphasizing the importance of segmentation methods.

DCE-MRI also faces other methodological challenges. For example, faster blood T_1 relaxation at 3 T can lead to perfusion overestimation if contrast dosing is not adjusted. To avoid this, Wu et al. halved the contrast dose [29]. Another challenge is the accuracy of the measurements with DCE. An inaccuracy can be affected by various factors such as the assumptions or measurement of the arterial input function and the choice of analysis model. Cutajar et al. implemented the Tofts model as an analysis method, which uses fixed parameter values such as the relax-

ivity of the contrast agent. These parameters are difficult to estimate accurately and introduce unreliability.

4.3. SNR and Repeatibility

A key advantage of ASL is its ability to repeatedly measure the renal perfusion without injection of a contrast agent. Among the included studies in this review, ASL generally demonstrated better repeatability than DCE-MRI. This is supported by lower CVs for ASL reported by Cutajar et al. and Wu et al. In addition to repeatability, image signal quality was reported in the form of SNR and tSNR values. The inconsistencies in reporting standards complicate direct comparison. Another important consideration is that a higher SNR does not necessarily mean a better measurement: Buchanan et al. showed that lower PWI-SNR techniques (e.g., SE-EPI) could still produce the highest tSNR. As the signal may fluctuate across time, tSNR is a more important parameter for quality assessment of the techniques.

4.4. Future Research

Although the literature on renal perfusion MRI has increased over time, this field requires further methodological and clinical development. Most importantly, there is still no true gold standard for renal tissue perfusion. This makes it challenging to validate the measurements of renal perfusion with ASL or DCE. The study by Alhummiany et al. attempted a clever workaround by using PC-MRI of renal artery flow as a reference point [1]. While this provided valuable insights (suggesting ASL and DCE are comparably accurate on average), PC-MRI does not measure the microvascular perfusion within the kidney. However, combining several imaging modalities could aid in the validation of the techniques.

Another shortcoming is that five of the studies had modest sample sizes, specifically under 20 subjects [4, 6, 10, 24, 29]. This limitation restricts the external validity of the findings. Although it is out of the scope of this review, only three of the included studies compared the techniques within patients with certain diseases (diabetics, CKD, and RCC) [1, 14, 24]. More research is needed to establish how ASL performs compared to other MRI techniques across a broader range of renal pathologies (transplant kidneys, renal artery stenosis, acute kidney injury, etc.).

Throughout the review, methodological variation is a recurring issue. To improve knowledge on renal perfusion MRI, imaging protocols such as those discussed in the PARENCHIMA consensus project should be used, and the variability within and between studies should be minimized as much as possible. This can be achieved by ensuring consistency in post-processing methods and subject preparation, such as hydration status, timing of imaging sessions, and the selection of similar patient populations.

5. CONCLUSION

ASL MRI is a non-invasive MRI technique with promising outcomes for measuring renal perfusion, particularly in populations where contrast agents are contraindicated. Compared to DCE-MRI, ASL reports lower perfusion values and better repeatability. However, variations in methodology, anatomy, and physiology across studies and individuals make comparison between DCE and ASL and within ASL difficult. Nevertheless, ASL has the potential to become a standard tool for renal perfusion assessment.

6. APPENDIX

6.1. Appendix A

The search strategy used in the PubMed database is: (("Renal Circulation" [mesh] OR "renal perfusion" [tw] OR "renal blood flow" [tw]) AND ("Magnetic Resonance Imaging" [mesh] OR "MR image" [tw] OR "MR image" [tw] OR "MR image" [tw] OR "arterial spin labeling" [tw] OR "arterial spin labeling" [tw] OR "arterial spin labeling" [tw] OR "dynamic contrast-enhanced MRI" [tw] OR "DCE-MRI" [tw] OR "intravoxel incoherent motion" [tw] OR "IVIM" [tw] OR "diffusion-weighted imaging" [tw] OR "DWI" [tw])).

The search strategy used in Embase is: ((*"Kidney Circulation"/ OR "kidney perfusion"/ OR "renal perfusion".ti,ab OR "kidney blood flow"/ OR "renal blood flow".ti,ab) AND (exp *"Nuclear Magnetic Resonance Imaging"/ OR "Magnetic Resonance Angiography"/ OR "MR image".ti,ab OR "MR image".ti,ab OR "MR image".ti,ab OR "arterial spin labeling".ti,ab OR "arterial spin labeling".ti,ab OR "dynamic contrast-enhanced MRI".ti,ab OR "DCE-MRI".ti,ab OR "intravoxel incoherent motion".ti,ab OR "IVIM".ti,ab OR "diffusion-weighted imaging".ti,ab OR "DWI".ti,ab) NOT (conference review or conference abstract).pt)

The search strategy used in the Web of Science database: ((TI=("Kidney Circulation" OR "kidney perfusion" OR "renal perfusion" OR "kidney blood flow" OR "renal blood flow") OR AK=("Kidney Circulation" OR "kidney perfusion" OR "renal perfusion" OR "kidney blood flow" OR "renal blood flow") OR AB=("Kidney Circulation" OR "kidney perfusion" OR "renal perfusion" OR "kidney blood flow" OR "renal blood flow")) AND (TI=("Nuclear Magnetic Resonance Imaging" OR "Magnetic Resonance Angiography" OR "MR image" OR "MR imag*" OR "arterial spin labeling" OR "arterial spin label*" OR "ASL" OR "dynamic contrast-enhanced MRI" OR "DCE-MRI" OR "intravoxel incoherent motion" OR "IVIM" OR "diffusion-weighted imaging" OR "DWI") OR AK=("Nuclear Magnetic Resonance Imaging" OR "Magnetic Resonance Angiography" OR "MR image" OR "MR imag*" OR "arterial spin labeling" OR "arterial spin label*"

OR "ASL" OR "dynamic contrast-enhanced MRI" OR "DCE-MRI" OR "intravoxel incoherent motion" OR "IVIM" OR "diffusion-weighted imaging" OR "DWI") OR AB=("Nuclear Magnetic Resonance Imaging" OR "Magnetic Resonance Angiography" OR "MR image" OR "MR image" OR "arterial spin labeling" OR "arterial spin label*" OR "ASL" OR "dynamic contrast-enhanced MRI" OR "DCE-MRI" OR "intravoxel incoherent motion" OR "IVIM" OR "diffusion-weighted imaging" OR "DWI")) NOT DT=(meeting abstract))

6.2. Appendix B

The NHLBI was adapted to assess the quality of the articles included in this systematic review to evaluate

Table 3: Quality assessment of selected studies based on nine methodological criteria

the included ASL MRI studies (Table 3). Four of the original 14 questions of the quality assessment tool for observational studies were included without modification (question 1, 2, 4, and 6), while the other four questions were modified. The remaining four questions were removed as they were not applicable to the included studies. Each article received 1 point for "Yes", and 0 points for "No", "Not Reported", or "Cannot Determine". Final scores were calculated as a percentage of applicable items. Studies were classified as "Great" for 75% or more, "Moderate" for 50-74%, or "Poor" for under 50% based on their total score.

Study	Q1	Q2	Q3	Q4	$\mathbf{Q5}$	$\mathbf{Q6}$	Q7	$\mathbf{Q8}$	Q 9	Classification
Alhummiany	/	1	Х	Х	1	✓	Х	Х	1	Moderate
Buchanan	✓	1	1	X	1	1	1	1	1	Great
Cutajar	✓	1	×	1	1	1	X	1	1	Great
Harteveld	✓	1	1	1	1	1	1	1	1	Great
Lu	✓	1	1	1	1	1	1	1	1	Great
Robson	✓	1	X	X	1	1	1	1	1	Great
Wu	✓	✓	X	✓	✓	✓	✓	✓	✓	Great

- Q1: Was the research question or objective clearly stated?
- **Q2:** Was the study population clearly specified and defined?
- Q3: Were any complications (e.g., motion artifacts, acquisition failure) reported?
- Q4: Were inclusion and exclusion criteria prespecified and applied uniformly?
- Q5: Was reproducibility assessed (e.g., ICC, intra-/interobserver reproducibility)?
- Q6: Were outcome measures (perfusion, SNR, reproducibility) clearly defined and applied consistently?
- Q7: Was image quality assessed quantitatively?
- **Q8:** Was there differentiation between renal regions (cortex vs. medulla)?
- **Q9:** Were relevant clinical or technical variables influencing perfusion reported?

Classification: Studies were classified as "Great" for 75% or more, "Moderate" for 50-74%, or "Poor" for under 50% based on their total score.

REFERENCES

- Alhummiany, B. A., Shelley, D., Saysell, M., et al. 2022, Journal of Magnetic Resonance Imaging, 55, 1241
- Broome, D. R. 2008, Investigative Radiology, 43, 830
- [3] Brown, R. S., Narayanan, M., Zhang, J. L., et al. 2019, Nephrology Dialysis Transplantation, 34, 929
- [4] Buchanan, C. E., Cox, E. F., and Francis, S. T. 2018, Diagnostics, 8, 43
- [5] Cai, Y.-Z., Li, Z.-C., Zuo, P.-L., et al. 2017, Journal of Magnetic Resonance Imaging, 46, 589
- [6] Cutajar, M., Thomas, D. L., Hales, P. W., et al.

- 2014, European Radiology, 24, 1300
- [7] Duhamel, G., Prevost, V., Girard, O. M., Callot, V., and Cozzone, P. J. 2014, Magnetic Resonance in Medicine, 71, 1186
- [8] Ferenbach, D. A. and Bonventre, J. V. 2015, The Journal of Physiology, 593, 3901
- [9] GBD Chronic Kidney Disease Collaboration. 2020, The Lancet, 395, 709
- [10] Harteveld, A. A., de Boer, A., Franklin, S. L., et al. 2020, Magnetic Resonance Materials in Physics, Biology and Medicine, 33, 81
- [11] Khalid, M. and Kahlon, M. U. 2021, Children, 8, 1123

- [12] Kidney Disease: Improving Global Outcomes (KDIGO) CKD Work Group. 2013, KDIGO 2012 Clinical Practice Guideline for the Evaluation and Management of Chronic Kidney Disease, KDIGO, available from: https://kdigo.org/wp-content/ uploads/2017/02/KDIGO_2012_CKD_GL.pdf
- [13] Kovesdy, C. P. 2022, Kidney International Supplements, 12, 7
- [14] Lu, F., Yang, J., Yang, S., et al. 2021, Journal of Magnetic Resonance Imaging, 54, 1152
- [15] Luis-Lima, S., Escamilla-Cabrera, B., Negrín-Mena, N., et al. 2019, Nephrology Dialysis Transplantation, 34, 287
- [16] Mao, W., Zhou, J., Zeng, M., et al. 2018, Magnetic Resonance Imaging, 45, 153
- [17] Meltzer, J. S. 2019, in Pharmacology and Physiology for Anesthesia: Foundations and Clinical Application, 2nd edn., ed. H. C. J. Hemmings and T. D. Egan (Elsevier), 782–794
- [18] Mora-Gutiérrez, J. M., Garcia-Fernandez, N., Roblero, M. F. S., et al. 2017, Journal of Magnetic Resonance Imaging, 46, 181
- [19] Nery, F., De Vita, E., Clark, C. A., Gordon, I., and Thomas, D. L. 2019, Magnetic Resonance in Medicine, 81, 2972
- [20] Nielles-Vallespin, S., de Boer, A., Blackledge, M., et al. 2020, Magnetic Resonance Materials in

- Physics, Biology and Medicine, 33, 131
- [21] Ouzzani, M., Hammady, H., Fedorowicz, Z., and Elmagarmid, A. 2016, Systematic Reviews, 5, 210
- [22] Porrini, E., Ruggenenti, P., Luis-Lima, S., et al. 2019, Nature Reviews Nephrology, 15, 177
- [23] Prince, M. R., Zhang, H. L., Chua-anusorn, W., et al. 2009, Journal of Magnetic Resonance Imaging, 30, 1298
- [24] Robson, P. M., Madhuranthakam, A. J., Smith, M. P., et al. 2016, Academic Radiology, 23, 144
- [25] Rossi, C., Artunc, F., Martirosian, P., et al. 2012, Investigative Radiology, 47, 490
- [26] Selcuk, A. 2019, Turkish Archives of Otorhinolaryngology, 57, 57
- [27] Villa, G., Ringgaard, S., Hermann, I., et al. 2019, Magnetic Resonance Materials in Physics, Biology and Medicine, 33, 885
- [28] Winter, J. D., St. Lawrence, K. S., and Cheng, H.-L. M. 2011, Journal of Magnetic Resonance Imaging, 34, 608
- [29] Wu, W.-C., Su, M.-Y., Chang, C.-C., Tseng, W.-Y. I., and Liu, K.-L. 2011, Radiology, 261, 845
- [30] Zhang, Q., Wang, D., Guo, Y., Duan, L., and Zhang, X. 2018, Abdominal Radiology, 43, 775
- [31] Zimmer, F., Nijssen, E. C., Gerlofs-Nijland, M. E., et al. 2013, Magnetic Resonance in Medicine, 69, 560